8-2022

# High-Precision CA-ID-TIMS U-Pb Zircon Geochronology of Felsic Rocks in the Finlayson Lake VMS District, Yukon: Linking Paleozoic Basin-Scale Accumulation Rates to the Occurrence of Subseafloor Replacement-Style Mineralization

Matthew J. Manor
*Memorial University of Newfoundland*

Stephen J. Piercey
*Memorial University of Newfoundland*

Corey J. Wall
*Boise State University*

Nikola Denisová
*Memorial University of Newfoundland*

# High-Precision CA-ID-TIMS U-Pb Zircon Geochronology of Felsic Rocks in the Finlayson Lake VMS District, Yukon: Linking Paleozoic Basin-Scale Accumulation Rates to the Occurrence of Subseafloor Replacement-Style Mineralization

Matthew J. Manor,[1,†] Stephen J. Piercey,[1] Corey J. Wall,[2,3] and Nikola Denisová[1]

[1]*Department of Earth Sciences, Memorial University of Newfoundland, St. John's, Newfoundland A1B 3X5, Canada*

[2]*Isotope Geology Laboratory, Department of Geosciences, Boise State University, Boise, Idaho 83725, USA*

[3]*Pacific Centre for Isotopic and Geochemical Research, Department of Earth, Ocean and Atmospheric Sciences, University of British Columbia, Vancouver, British Columbia V6T 1Z4, Canada*

## Abstract

Felsic igneous complexes and associated volcano-sedimentary rocks in continental back-arc environments host large-tonnage and/or high-grade volcanogenic massive sulfide (VMS) deposits. The emplacement mechanisms, style, and preservation of these deposits is thought to be partially dependent on depositional rates of the host lithofacies (i.e., discrete volcanic eruptions) relative to the setting of massive sulfide genesis on the seafloor as mounds and/or via subseafloor replacement of existing strata. The localization and occurrence of subseafloor replacement-style VMS deposits is therefore strongly influenced by the characteristics of the volcano-sedimentary facies in the hosting basin and the rates of their emplacement; the latter are poorly constrained in the literature due to the difficulty of obtaining high-precision dates that make this possible in Phanerozoic and older rocks. New high-resolution U-Pb geochronology and detailed regional stratigraphic investigation indicate that Devonian-Mississippian volcanic rocks and associated VMS mineralization in the Yukon-Tanana terrane in the Finlayson Lake district, Yukon, Canada, were erupted or emplaced during distinct time periods (ca. 363.3, 362.8, and 355.2 Ma) in two discrete submarine basins: the Kudz Ze Kayah formation and the Wolverine Lake group. The VMS deposits in both settings are contained within intrabasinal rocks that accumulated at rapid rates of ~350 to 2,000 m/m.y. over 0.6 to 1.4 m.y. Locally, these rates reach peak rates up to 7,500 m/m.y. in the Wolverine Lake group, which are interpreted to reflect facies deposition by mass transport complexes or turbidity currents. These new dates indicate that rapid accumulation of volcanic rocks in the back-arc basins was critical for localizing subseafloor replacement-style mineralization and the development of the Zn-enriched GP4F, Kudz Ze Kayah, and Wolverine VMS deposits. Rapid depositional processes observed in these deposits and their host basins are interpreted to have an important role in developing highly porous and permeable, water-saturated lithofacies that provide optimal conditions for enhancing zone refining processes and subsequent preservation of massive sulfide mineralization, which are key in the development of high-grade and large-tonnage VMS deposits. It is herein suggested that quantitative basin-scale accumulation rates, as a result of new U-Pb geochronological methods and increased precision combined with detailed stratigraphic and facies analysis, may provide important perspectives on the formation of continental back-arc basins and the localization of VMS deposits in other continental margin environments globally.

## Introduction

Silicic magmatism at convergent margins contributes to the growth of continental crust and drives the formation of hydrothermal ore deposits in both the arc (e.g., porphyry Cu deposits; Sillitoe, 2010) and back-arc environments (e.g., volcanogenic massive sulfide [VMS] deposits; Franklin et al., 2005; Piercey, 2011). In the back-arc environment, slab rollback, crustal extension, and upwelling of asthenosphere-derived melts elevate the geothermal gradient, increase heat flow, and enhance fluid circulation in the upper crust (McKenzie and Bickle, 1988; Heuret and Lallemand, 2005). Extensional faults within the back-arc rifts facilitate magma transport in the crust and the formation of subvolcanic intrusions, volcanic flows, or explosive pyroclastic eruptions on the seafloor (Gibson et al., 1999). Rapid accumulation of volcanic-subvolcanic

facies (± epiclastic sedimentary rocks) in the subaqueous environment of continental back-arc basins provides insight into the nature of volcanism, sedimentation, and subsidence in ancient seafloor environments. Collectively, volcanic and volcano-sedimentary rock emplacement style can also influence the styles of VMS mineralization. Flow-dominated environments commonly lead to exhalative mound development (i.e., black smoker chimneys), whereas in more clastic-dominated environments, replacement-style deposits are common where sulfides replace porous and, to a lesser extent, coherent volcanic and sedimentary facies (e.g., Franklin et al., 2005; Gibson, 2005). Rapid accumulation of volcaniclastic rocks in VMS settings has been proposed as an important aspect of forming large and/or high-grade VMS deposits in the subseafloor environment (e.g., Doyle and Allen, 2003). However, despite the potential tectonic and economic importance of emplacement rates at which volcanic facies are accumulated, the rates, how they are related to the formation and localization of VMS de-

[†]Corresponding author: e-mail, mjmanor@mun.ca

posits, and their role in facilitating subseafloor replacement mineralization remain poorly understood.

Deciphering rates of volcanic and sediment accumulation in the ancient rock record is challenging due to the paucity of robust geochronological data in ancient assemblages. Further, most historical geochronological data, or dates obtained by less precise in situ methods (e.g., laser ablation-inductively coupled plasma-mass spectrometry [LA-ICP-MS] or secondary ion mass spectrometry [SIMS]), are not sufficient for robust calculations of ancient emplacement rates at the resolution required to investigate VMS formation. Thus, determining volcanic emplacement rates requires the application of modern, high-precision geochronological methods, such as chemical abrasion-isotope dilution-thermal ionization mass spectrometry (CA-ID-TIMS) U-Pb zircon geochronology (Mattinson, 2005) and precise controls on stratigraphic and structural relationships for the VMS-hosting rock packages (e.g., Bleeker et al., 1999; Ross et al., 2014; Oliver et al., 2021). Current U-Pb zircon geochronological methods allow for a precision of <0.1% on single zircon crystals with weighted mean dates that can decipher distinct Paleozoic magmatic events less than 100 k.y. apart (Schoene and Baxter, 2017). Utilizing modern CA-ID-TIMS methods, we present the first set of new high-precision U-Pb zircon dates for mid-Paleozoic back-arc related rocks in the Kudz Ze Kayah formation and Wolverine Lake group in the Finlayson Lake VMS district, Yukon, Canada, which together contain >25 Mt of polymetallic base metal sulfide resources (Regan, 2007; Peter et al., 2007; van Olden et al., 2019). The rock packages in this district are interpreted to be deposited in relatively small (<600 km$^2$), restricted continental back-arc basins that formed along the western margin of ancestral North America in the Late Devonian to Early Mississippian (e.g., Bradshaw et al., 2008). We integrate stratigraphic data and, to our knowledge, the highest-resolution U-Pb results ever reported for any VMS district in the ancient geologic record to calculate linear and volumetric, time-resolved accumulation rates for volcanic and sedimentary rock assemblages within the Finlayson Lake VMS district. These calculated rates indicate rapid accumulation of large volumes of subaqueous volcanic and sedimentary facies during the early back-arc rifting stage. The results may indicate a possible link between rapid, basin-scale volcano-sedimentary processes and the localization and genesis of Zn-rich, replacement-style VMS deposits in the Finlayson Lake district.

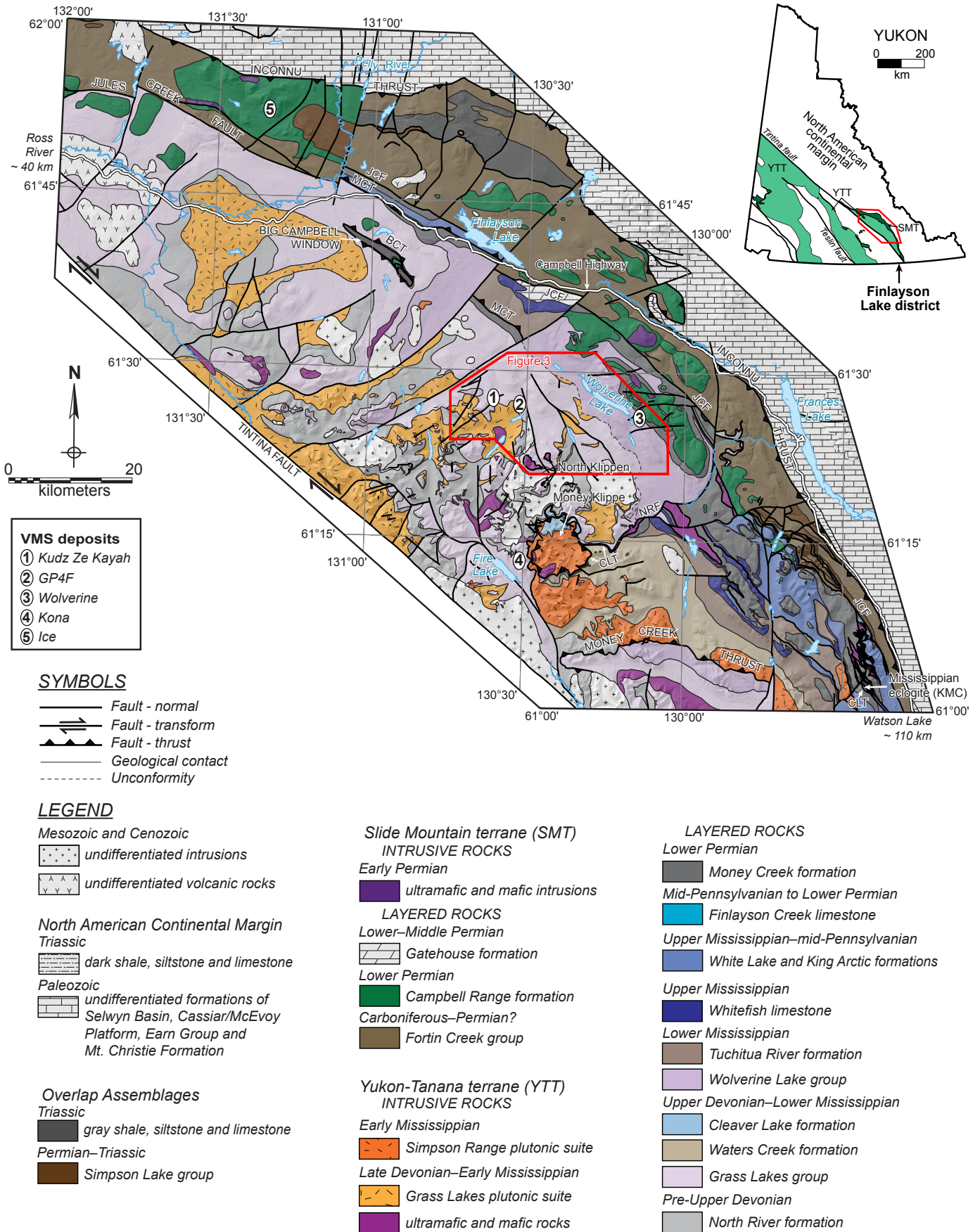## Geologic and Stratigraphic Setting

The Finlayson Lake VMS district, Yukon, Canada, is a fault-bounded portion of the Yukon-Tanana and Slide Mountain terranes that formed adjacent to the peri-Laurentian continental margin in the mid- to late-Paleozoic (Fig. 1; Tempelman-Kluit, 1979; Mortensen and Jilson, 1985; Murphy et al., 2006). Rocks that compose the Yukon-Tanana terrane arc and back-arc assemblages are volcanic, plutonic, and sedimentary rocks that were deposited above or intruded a pre-Late Devonian basement; these rocks are variably deformed and metamorphosed but locally retain primary geologic and geochemical features (Colpron et al., 2006; Murphy et al., 2006; Piercey et al., 2006; Piercey and Colpron, 2009). The Jules Creek transform fault juxtaposes rocks of the Yukon-Tanana terrane with ophiolitic rocks of the Slide Mountain terrane (Figs. 1, 2; Murphy et al., 2006), which were then together thrust above North American platformal strata along the Inconnu thrust in the Late Jurassic (Murphy et al., 2002). In the Eocene, Yukon-Tanana terrane rocks were displaced ~430 km along the Tintina strike-slip dextral fault system, resulting in the Finlayson Lake district (Fig. 1; Gabrielse et al., 2006).

Yukon-Tanana terrane rocks within the Finlayson Lake VMS district are hosted in three distinct structurally imbricated panels (from deepest to shallowest): the Big Campbell, Money Creek, and Cleaver Lake thrust sheets (Figs. 1, 2; Murphy et al., 2006). We will only discuss the geology of the Big Campbell thrust sheet in the scope of this paper, as the Money Creek and Cleaver Lake thrust sheets contain no known VMS mineralization; we refer the reader to Murphy et al. (2006) for descriptions of these rock packages. The Big Campbell thrust sheet is bounded below by the post-Late Triassic Big Campbell thrust fault and above by the Early Permian Money Creek thrust fault (Figs. 1, 2). Rocks in the Big Campbell thrust sheet include the basal Upper Devonian metasedimentary rocks of the North River formation overlain by Upper Devonian mafic and felsic metavolcanic and metasedimentary rocks of the Grass Lakes group, which include the Fire Lake, Kudz Ze Kayah, and Wind Lake formations (Figs. 1, 2). Late Devonian gabbroic to dioritic intrusions of the North Lakes intrusion and granitoid intrusions of the Grass Lakes plutonic suite cut the Grass Lakes group. The Grass Lakes group is unconformably overlain by Lower Mississippian metaclastic and mafic to felsic metavolcanic rocks of the Wolverine Lake group (Figs. 1–3). Metasedimentary rocks of the Lower Permian Money Creek formation are interpreted to unconformably overlie the Wolverine Lake group. Bimodal felsic and felsic-siliciclastic Zn-enriched VMS mineralization in the Big Campbell thrust sheet is present throughout the Grass Lakes group stratigraphy (GP4F and Kudz Ze Kayah deposits; Piercey et al., 2001; Sebert et al., 2004; Peter et al., 2007) and in the Wolverine Lake group (Wolverine deposit; Bradshaw et al., 2008; Figs. 1–4); mafic-siliciclastic VMS mineralization is present in the Fire Lake formation (Kona Cu-Co deposit; Sebert et al., 2004; Peter et al., 2007). Rocks and associated VMS mineralization in the Grass Lakes and Wolverine Lake groups are interpreted to have formed in an evolving continental arc to back-arc basin environment that represents the earliest stages of rifting on the western peri-Laurentian continental margin (Piercey et al., 2001, 2002, 2004, 2006; Murphy et al., 2006).

Our discussion below focuses on the felsic VMS-bearing assemblages in the Big Campbell thrust sheet that have been

Fig. 1. Regional geologic setting of the Finlayson Lake district, Yukon-Tanana terrane, Yukon (modified after Murphy et al., 2006 and Colpron and Nelson, 2011). Numbers indicate locations of VMS deposits in the region. Abbreviations: BCT = Big Campbell thrust, CLT = Cleaver Lake thrust, JCF = Jules Creek fault, MCT = Money Creek thrust, NRF = North River fault, VMS = volcanogenic massive sulfide. Inset map of Yukon shows the distribution of Paleozoic terranes (YTT = Yukon-Tanana terrane; SMT = Slide Mountain terrane) relative to the North American continental margin.

**VMS deposits**
1. Kudz Ze Kayah
2. GP4F
3. Wolverine
4. Kona
5. Ice

**SYMBOLS**
- Fault - normal
- Fault - transform
- Fault - thrust
- Geological contact
- Unconformity

**LEGEND**

**Mesozoic and Cenozoic**
- undifferentiated intrusions
- undifferentiated volcanic rocks

**North American Continental Margin**
Triassic
- dark shale, siltstone and limestone
Paleozoic
- undifferentiated formations of Selwyn Basin, Cassiar/McEvoy Platform, Earn Group and Mt. Christie Formation

**Overlap Assemblages**
Triassic
- gray shale, siltstone and limestone
Permian–Triassic
- Simpson Lake group

**Slide Mountain terrane (SMT)**
INTRUSIVE ROCKS
Early Permian
- ultramafic and mafic intrusions
LAYERED ROCKS
Lower–Middle Permian
- Gatehouse formation
Lower Permian
- Campbell Range formation
Carboniferous–Permian?
- Fortin Creek group

**Yukon-Tanana terrane (YTT)**
INTRUSIVE ROCKS
Early Mississippian
- Simpson Range plutonic suite
Late Devonian–Early Mississippian
- Grass Lakes plutonic suite
- ultramafic and mafic rocks

**LAYERED ROCKS**
Lower Permian
- Money Creek formation
Mid-Pennsylvanian to Lower Permian
- Finlayson Creek limestone
Upper Mississippian–mid-Pennsylvanian
- White Lake and King Arctic formations
Upper Mississippian
- Whitefish limestone
Lower Mississippian
- Tuchitua River formation
- Wolverine Lake group
Upper Devonian–Lower Mississippian
- Cleaver Lake formation
- Waters Creek formation
- Grass Lakes group
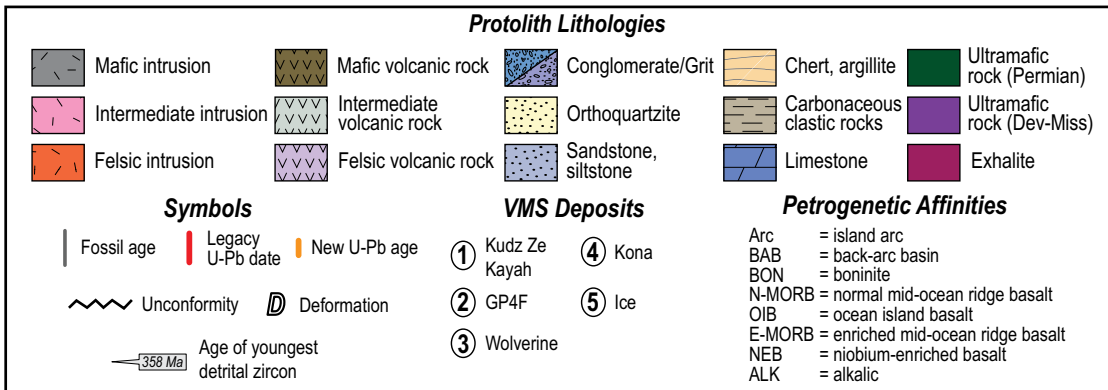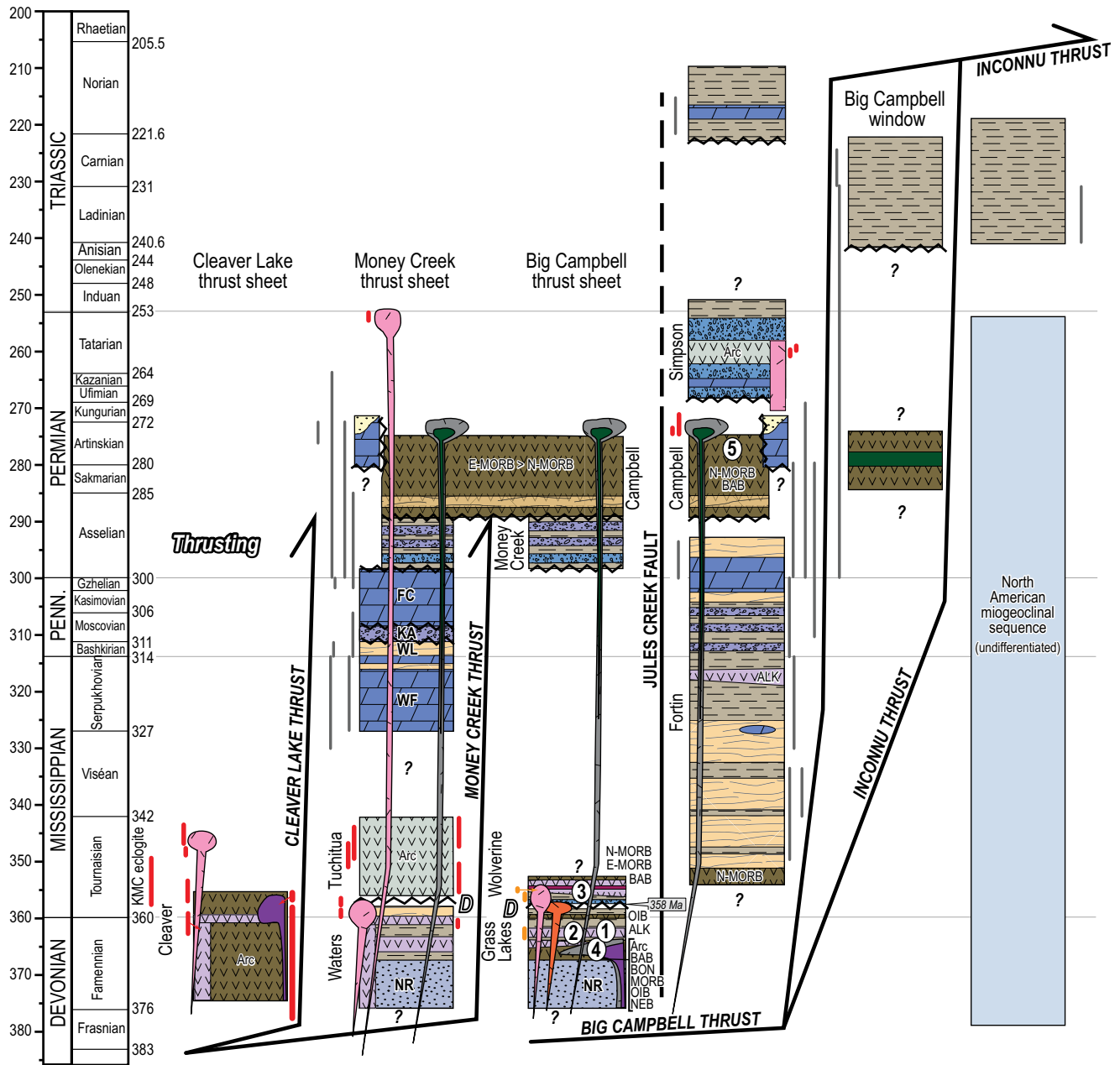Pre-Upper Devonian
- North River formation

Fig. 2. Composite chronostratigraphic columns for the Finlayson Lake district with locations of VMS prospects, U-Pb zircon and fossil ages, and petrogenetic affinities (modified after Murphy et al., 2006). Abbreviations: KMC = Klatsa Metamorphic Complex, NR = North River formation, Penn. = Pennsylvanian.
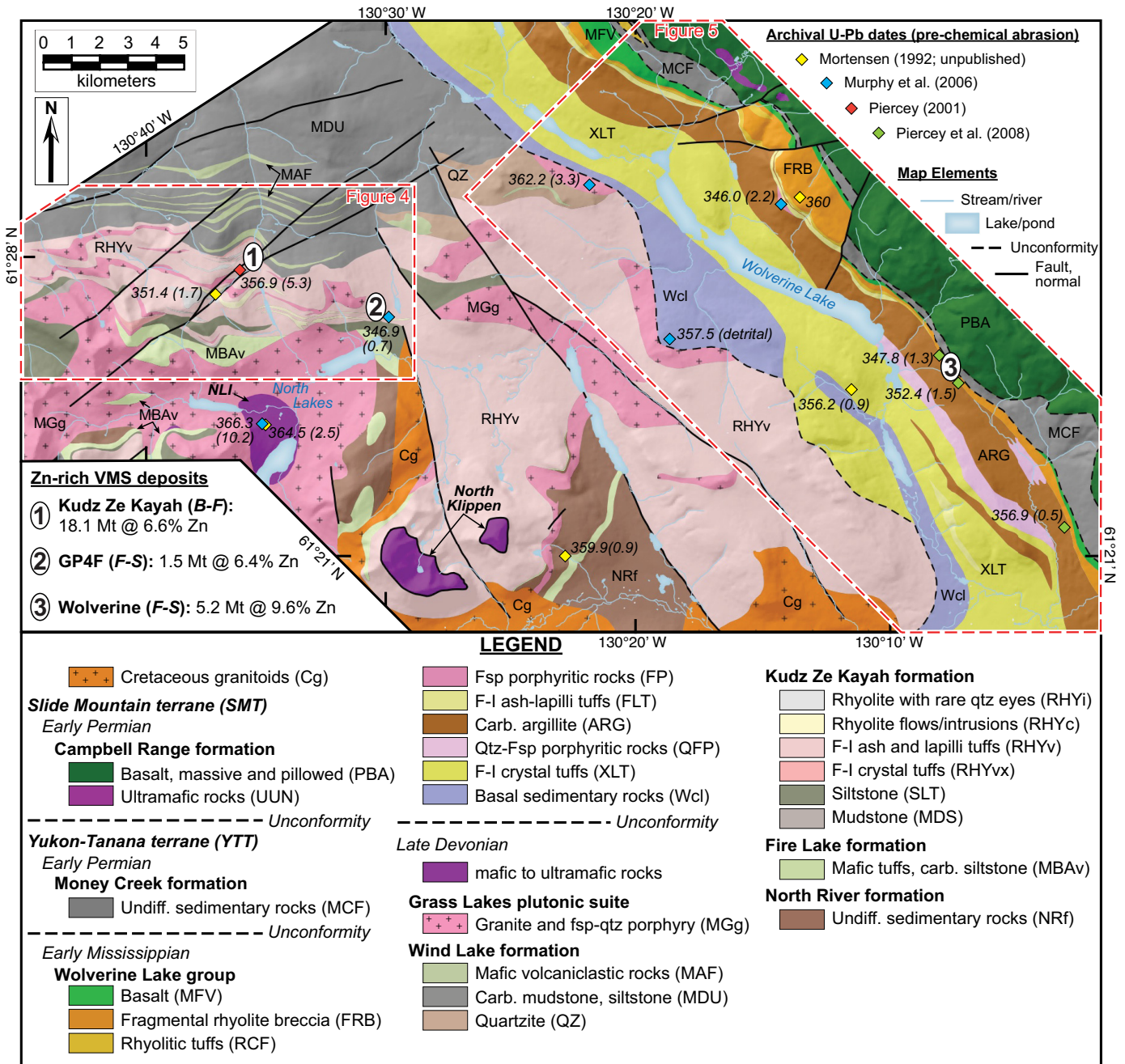
Fig. 3. Geologic setting of the Kudz Ze Kayah formation and Wolverine Lake group illustrating property-scale mapping from this study merged with regional data sets (after Yukon Geological Survey, 2018; van Olden et al., 2019). Circled numbers correspond to Zn-rich volcanogenic massive sulfide (VMS) deposits in felsic stratigraphy after Figures 1 and 2. Diamond symbols show locations of archival U-Pb dates, where colors correspond to study reference. Numbers in parentheses are the 2s uncertainty on the U-Pb date in Ma. Red box outlines correspond to zoomed in maps in Figures 4 and 5. Abbreviations: B-F = bimodal-felsic VMS deposit, carb = carbonaceous, F = felsic, F-S = felsic-siliciclastic VMS deposit, Fsp = feldspar, I = intermediate, Qtz = quartz.

variably metamorphosed to greenschist facies (Murphy et al., 2006). However, primary textures are preserved throughout the rock units in the Grass Lakes and Wolverine Lake groups (e.g., lapilli, laminations), and as such, we omit the prefix "meta" from all rock descriptions below. Descriptive terminology is used for coherent and volcaniclastic lithofacies (i.e., tuff, lapilli tuff, aphyric) that follows the non-genetic, size-based nomenclature of Fisher (1966), recently updated by White and Houghton (2006).

*Lithostratigraphy of the Kudz Ze Kayah formation and Wolverine Lake group*

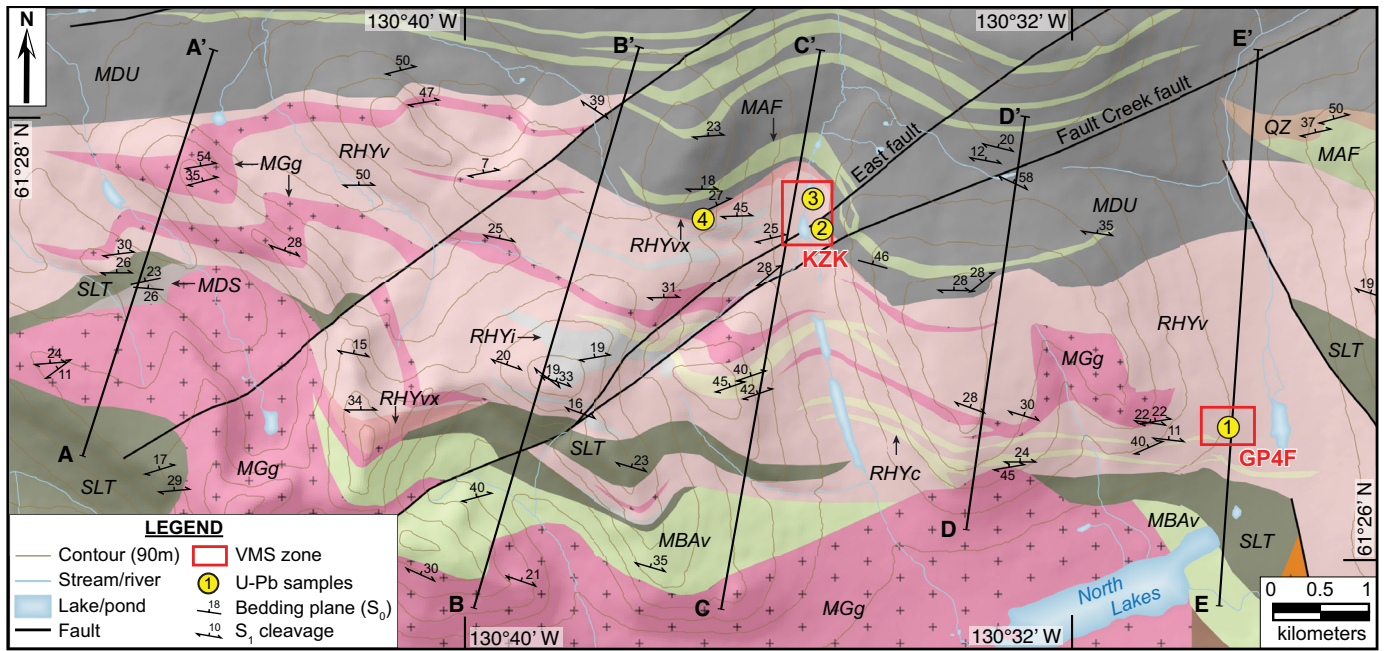The Kudz Ze Kayah formation and Wolverine Lake group contain the greatest abundance of back-arc related felsic

Fig. 4. Geologic map of the Kudz Ze Kayah formation (after van Olden et al., 2019) showing U-Pb geochronology sample locations (yellow circles and black numbers) and lines of cross section lines used to reconstruct stratigraphic sections. Structural data is shown for representative measurements used to construct cross sections for $S_0$ and $S_1$ cleavages only. Red boxes correspond to VMS zones. Unit labels and colors as in Figure 3.
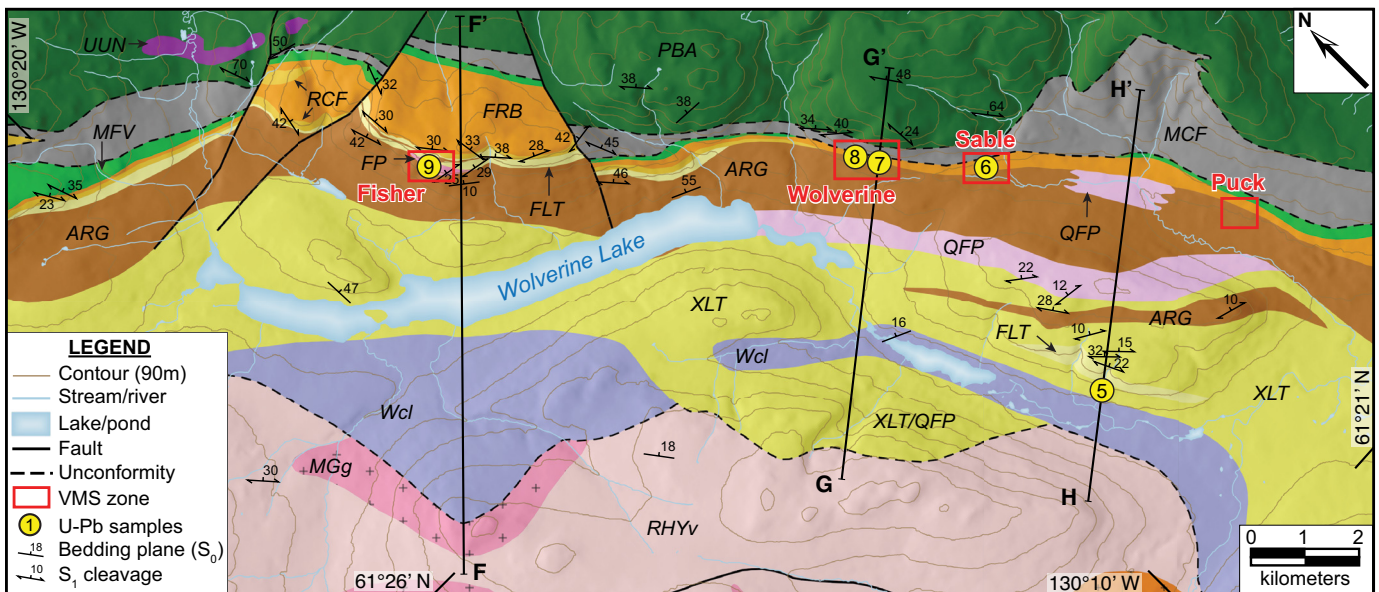


Fig. 5. Geologic map of the Wolverine Lake group, merged with regional mapping (after Yukon Geological Survey, 2018). Symbols and labels as in Figures 3 and 4.

volcanic facies in the Finlayson Lake district (Piercey et al., 2001), were deposited in two distinct continental margin basins, and both contain multiple occurrences of sulfide mineralization (e.g., Figs. 1–3; Peter et al., 2007). Geologic mapping, cross sections, and stratigraphic reconstructions indicate that both stratigraphic units are characterized by lateral variations in thickness over minimum strike lengths of ~15 km (Kudz Ze Kayah formation) and ~23 km (Wolverine Lake group; Figs. 3–8). The lower part of the Kudz Ze Kayah stratigraphy

consists of siltstone and carbonaceous argillite (~130–500 m thick), but volcaniclastic rocks (i.e., tuffs, lapilli tuffs, and crystal tuffs), aphanitic rhyolitic intrusive rocks, and minor mudstone and mafic intrusive rocks compose the remaining ~400 to 1,300 m of stratigraphy throughout the district (Figs. 4, 6, 8). The volcaniclastic rocks (RHYv; Fig. 9A-D) are volumetrically dominant and contain facies variations that are indistinguishable at the regional scale; these variations occur both along strike and up-section but are mapped as one regional
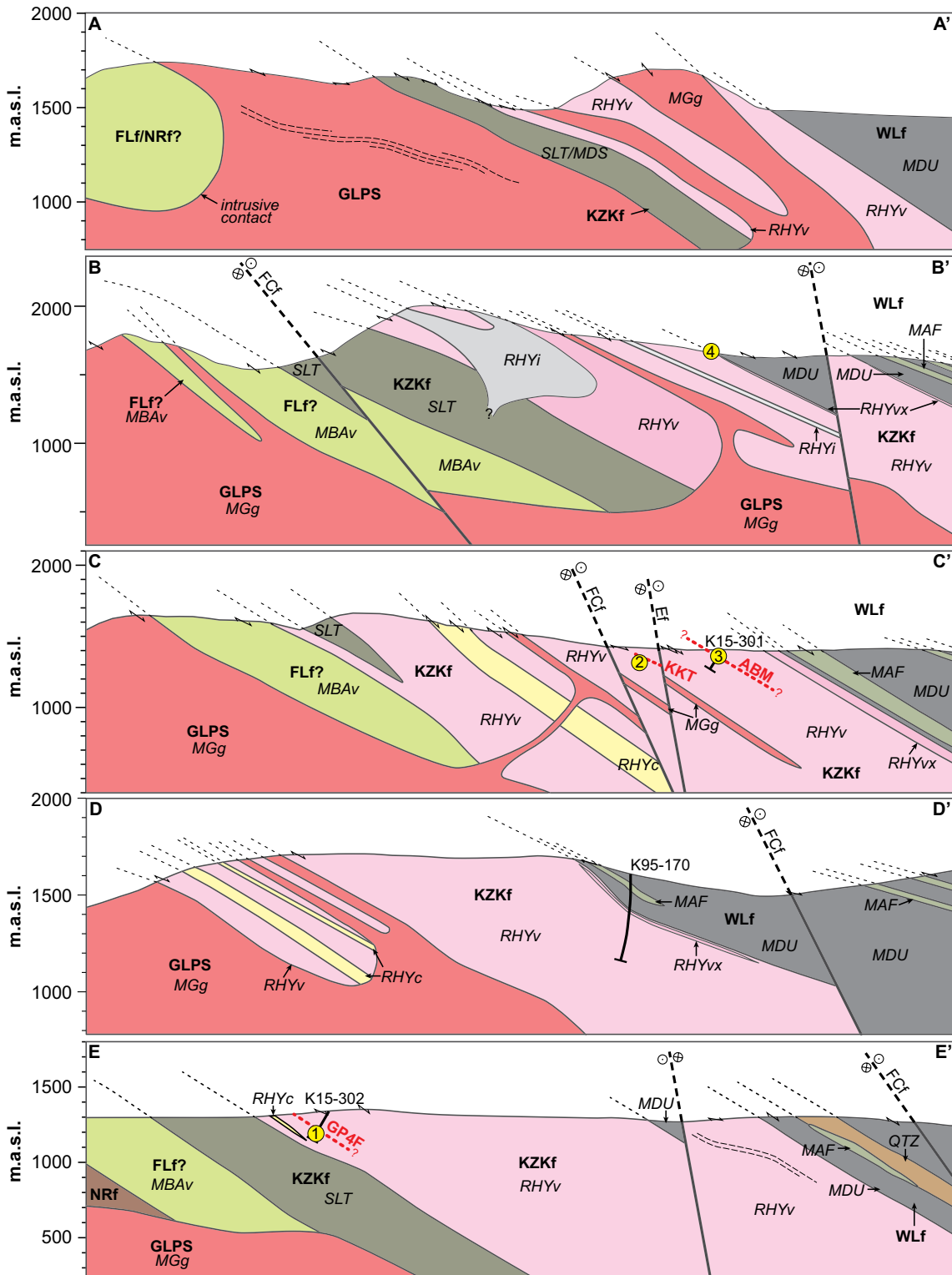
Fig. 6. Cross sections for lines A-A', B-B', C-C', D-D', and E-E' in the Kudz Ze Kayah formation, drafted with no vertical exaggeration. Sections correspond to plan view lines in Fig. 4. Unit colors and abbreviations as in the legend in Fig. 3. U-Pb samples are shown as yellow circles for reference and projected into the cross section where applicable (B-B' and C-C'; 17MM-002); numbers correspond to sample symbols in Figures 4 and 5. Thin, black dashed lines in the subsurface are interpreted cleavage plane variations based on outcrop measurements. Red dashed lines indicate approximate location of VMS lenses. Arrows on the surface indicate locations of outcrop measurements corrected as apparent dips. Abbreviations: Ef = East fault, FCf = Fault Creek fault, FLf = Fire Lake formation, GLPS = Grass Lakes plutonic suite, KKT = Krakatoa, KZKf = Kudz Ze Kayah formation, NRf = North River formation, WLf = Wind Lake formation.
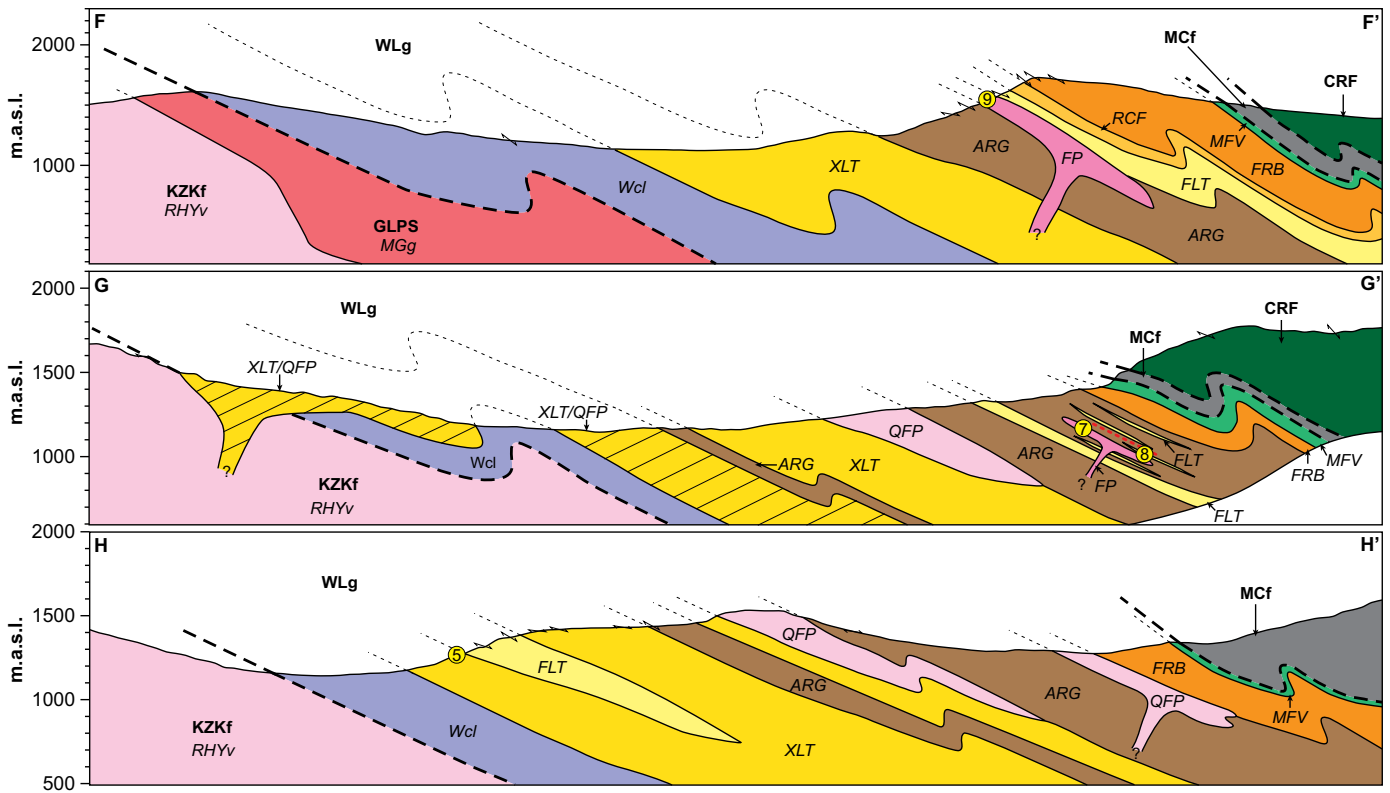
Fig. 7. Cross sections for lines F-F', G-G', and H-H' in the Wolverine Lake group, drafted with no vertical exaggeration. All aspects of cross sections the same as in Fig. 6. Abbreviations: CRF = Campbell Range formation, MCf = Money Creek formation, WLg = Wolverine Lake group.

geologic unit (Fig. 4). Coherent rhyolites (RHYc; Fig. 9E, F) are present as discrete units that crop out over a 6-km strike length and have been transposed subparallel to the regional S₁ cleavage (Fig. 4). These rocks are spatially associated with aphyric rhyolites that contain minor quartz eyes (RHYi), and both RHYc and RHYi units exhibit features that are indicative of being stratigraphically concordant; however, surface expressions of the RHYi unit are limited to between the B-B' and C-C' cross sections (<2 km along strike; e.g., Figs. 4, 6). Tuffaceous facies are commonly poorly sorted and, where lapilli and/or crystals are present, are matrix- to clast-supported (e.g., Fig. 9B, C) with random grain sizes and modal distributions; rare instances of graded bedding within the tuffs are present. In the Kudz Ze Kayah formation, massive sulfides are present in the felsic-siliciclastic GP4F deposit (1.5 Mt at 6.4% Zn, 3.1% Pb, 0.1% Cu, 2.0 g/t Au, and 81.7 g/t Ag; MacRobbie and Holroyd, 2000), located ~70 m above the siltstone-volcaniclastic facies transition in the lower Kudz Ze Kayah formation, and in the bimodal-felsic Kudz Ze Kayah deposit (18.1 Mt at 6.6% Zn, 2.0% Pb, 0.9% Cu, 1.4 g/t Au, and 156 g/t Ag; van Olden et al., 2019)—consisting of the ABM and Krakatoa zones—located higher in the Kudz Ze Kayah stratigraphy, ~500 to 600 m above GP4F (Fig. 4; Peter et al., 2007). Coarse grained, alkali feldspar porphyritic granites and sills of the Grass Lakes plutonic suite intrude the Kudz Ze Kayah formation and overlying Wind Lake formation, providing a minimum age for the latter rocks (Fig. 4).

The Wolverine Lake group contains a basal unit of quartzofeldspathic grit and conglomerate (~170–470 m; ca. 357.5 Ma;

Murphy et al., 2006) that is overlain by a thick footwall sequence (~500–1,000 m) of crystal-rich volcaniclastic rocks and intercalated tuffs and argillites that are interpreted to have commenced deposition by ca. 356.2 Ma (Figs. 5, 7, 8; Murphy et al., 2006). The crystal tuffs in this sequence (XLT) are generally more homogeneous than in the Kudz Ze Kayah formation, and at a regional scale, the fine-grained tuffs occur as distinct bedforms within the crystal tuff unit (Fig. 5). These rocks are gradationally overlain by carbonaceous argillite that is intruded or interbedded with felsic porphyritic and volcaniclastic rocks, respectively (~700 m; Fig. 9G-I). Mineralization is present near the top of the footwall sequence as the felsic-siliciclastic Wolverine deposit (Wolverine and Lynx zones; 5.2 Mt at 9.66% Zn, 1.26% Pb, 0.91% Cu, 281.8 g/t Ag; Regan, 2007) and the Puck, Sable, and Fisher zones (Fig. 5; Bradshaw et al., 2008; Piercey et al., 2008). Fine-grained resedimented rhyolitic tuff/siltstone, carbonate and quartz-pyrite exhalite, iron formation, shale, greywacke, and MORB-type basalts comprise Wolverine Lake group hanging-wall facies (~150–460 m); all of these facies represent a sharp geochemical transition from facies of the Wolverine Lake group footwall (Figs. 5, 8; Piercey et al., 2001, 2016; Bradshaw et al., 2008).

### Structure

Rocks in the Grass Lakes and Wolverine Lake groups have been metamorphosed to greenschist facies and exhibit four phases of deformation (e.g., Fig. 10; Murphy and Piercey, 1999; Murphy et al., 2006). In both areas, local occurrences of fine laminations in argillite define primary bedding planes
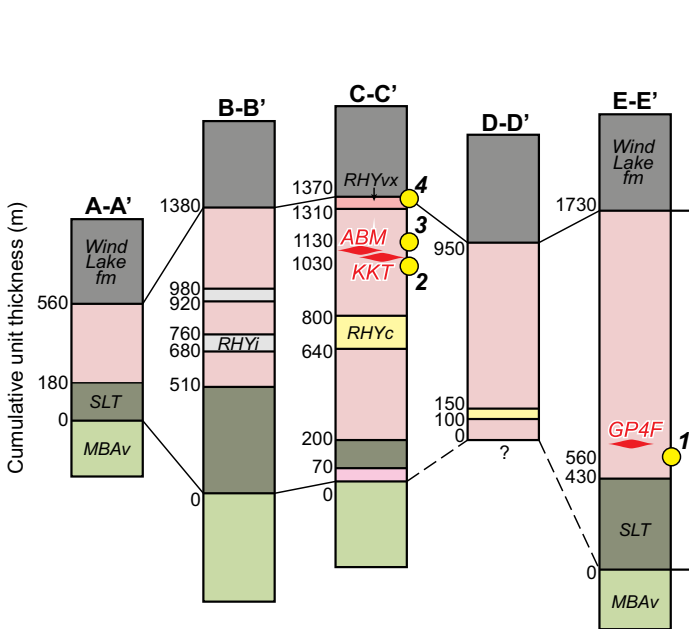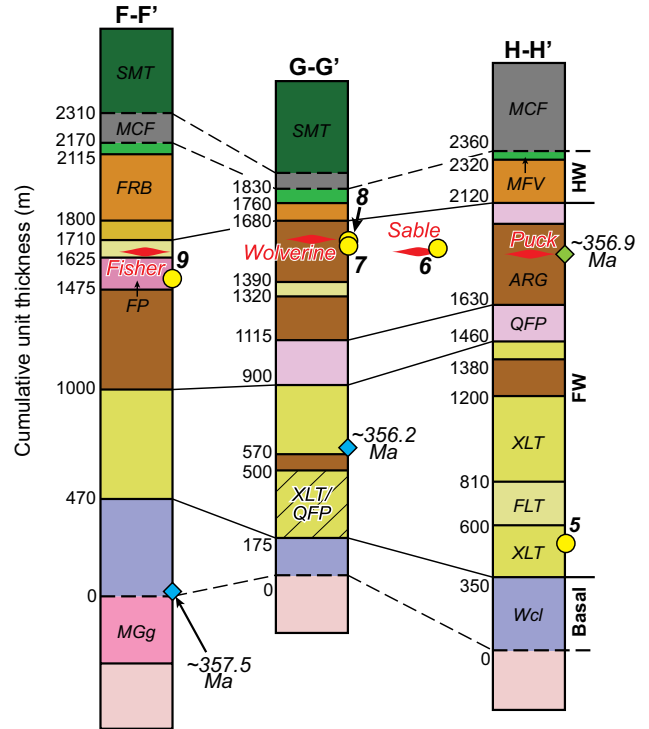
Fig. 8. Regional stratigraphic columns for A) Kudz Ze Kayah formation, and B) the Wolverine Lake group. Columns show cumulative unit thicknesses, approximate locations of VMS deposits, and U-Pb sample locations (circles = this study; diamonds = data from Murphy et al., 2006; Piercey et al., 2008). Unit thicknesses are measured from interpreted cross sections in Figures 6 and 7. Thicknesses in panel (A) account for fault restoration and subtraction of Grass Lakes plutonic suite granites, as these rocks intruded the volcanic succession following the transition into the overlying Wind Lake formation. Thick dashed lines in the columns represent unconformities; solid lines are locations of facies changes. Bold numbers correspond to sample numbers in Figures 4 and 5. Abbreviations: FW = footwall, HW = hanging wall, KKT = Krakatoa VMS zone. Unit colors correspond to Figure 1.

($S_0$; e.g., Fig. 10C). The first deformation ($D_1$) is represented by penetrative foliation in the Grass Lakes group ($S_{1-GLg}$) that is typically subparallel to the $S_0$ bedding planes and is defined by oriented micas, flattened lapilli and feldspar crystals, and fissile argillite (e.g., Figs. 9, 10). The $D_1$ structures are interpreted to result from the regional deformation event at ca. 358 Ma (Murphy and Piercey, 1999; Murphy et al., 2006). A second phase of deformation ($D_2$) is recognized by the following: 1) local crenulation fabrics ($S_{2-GLg}$) in the Grass Lakes group that are oblique to the $S_{1-GLg}$ in rocks with low competency (e.g., argillite and sericite-altered, well-foliated volcaniclastic rocks; Fig. 10B); 2) rare, mesoscale folds that contain the $S_0$ and $S_{1-GLg}$ foliation ($F_{1-GLg}$); 3) penetrative foliation in the Wolverine Lake group ($S_{1-WLg}$) that is subparallel to bedding in argillite ($S_0$), represented by similar oriented mica, feldspar, and lapilli as in the Grass Lakes group; and 4) a weakly foliated, discordant granitic intrusion that cuts previously deformed ($S_{1-GLg}$) argillites in the Wind Lake formation (Murphy et al., 2006). The $D_1$ and $D_2$ deformations are further supported by distinct $S_{1-GLg}$ (~20°–30° dip to the northnortheast) and $S_{1-WLg}$ (~20°–30° dip to the east) that define the dominant penetrative foliation in the Grass Lakes group and Wolverine Lake group, respectively. The third deformation phase ($D_3$) is present primarily as localized, southwestvergent isoclinal folds ($F_{1-WLg}$) in the upper Wolverine Lake

group footwall and hanging wall (mm- to m-scale) that fold the earlier $S_{1-WLg}$ fabric. The orientation of these $F_{1-WLg}$ folds together with E-dipping $S_{1-WLg}$ cleavage supports earlier hypotheses that the Wolverine Lake group stratigraphy makes up part of the eastern limb of an open, upright, N-NE–trending, regional anticline (Murphy and Piercey, 1999; Bradshaw et al., 2008). Stratigraphically above the Wolverine Lake group in the Campbell Range formation basalts, tight isoclinal anticline-syncline pairs have been interpreted as the areas of highest strain during the $D_3$ deformation which are considered to be near a synclinal hinge of the regional anticline (Murphy and Piercey, 1999). Finally, the latest deformation ($D_4$) is represented by late, brittle faults in two orientations: 1) NE-E–trending structures that cut both the Grass Lakes and Wolverine Lake groups with ~320 m of mappable offset (e.g., East and Fault Creek faults; Figs. 4, 5) and 2) N-NW–trending structures in the Grass Lakes group (Fig. 3; Murphy and Piercey, 1999).

*Unit thickness corrections and assumptions*

The unit thicknesses for lithofacies in the Kudz Ze Kayah formation and Wolverine Lake group can be estimated despite deformation in the Big Campbell thrust sheet. We base this interpretation on the following arguments. First, argillites in both the Grass Lakes and Wolverine Lake groups contain
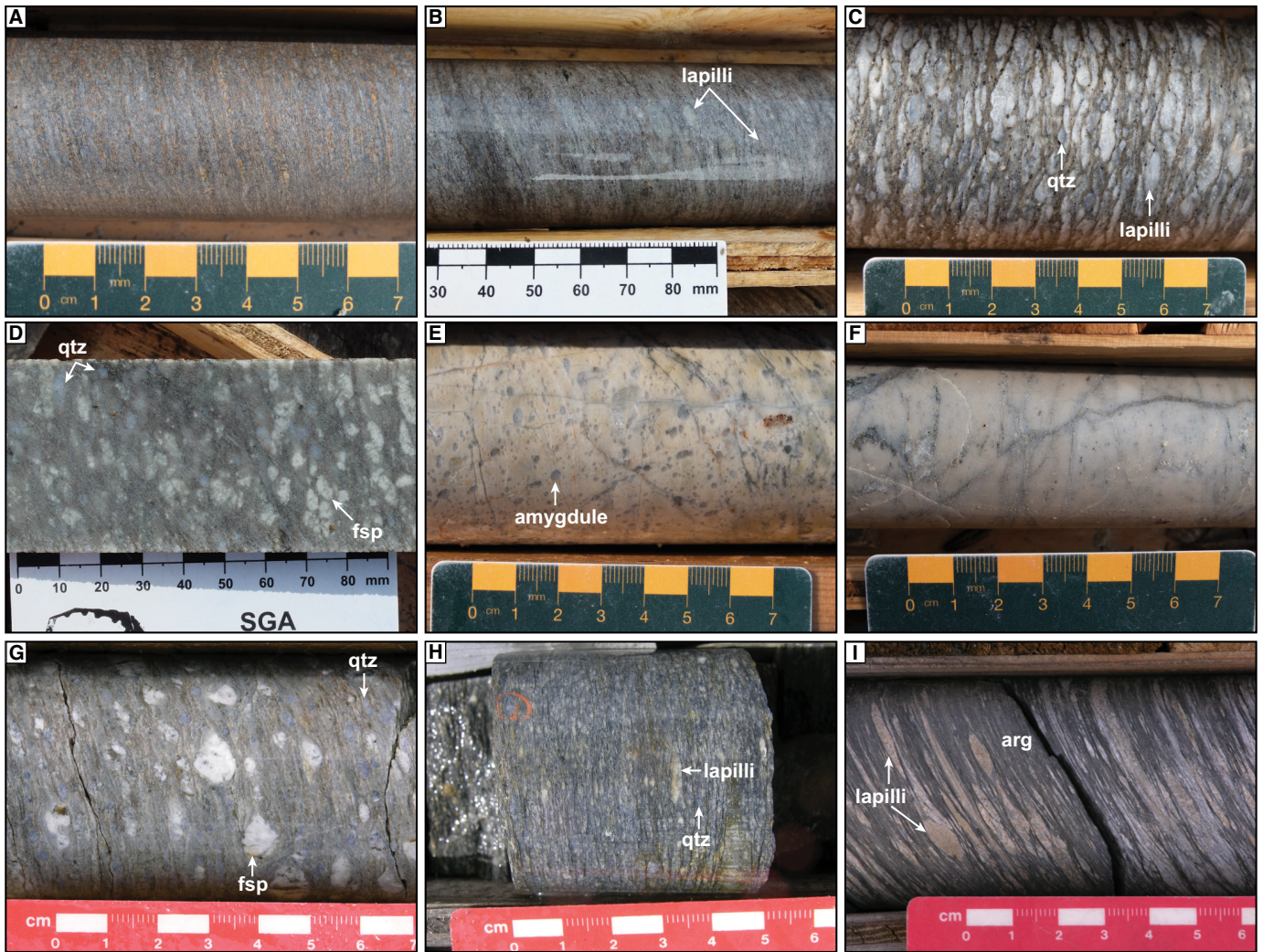
Fig. 9. Representative volcanic lithofacies in the Kudz Ze Kayah formation (A-F) and the Wolverine Lake group footwall (G-I). A) felsic tuff; B) matrix-supported felsic lapilli tuff; C) clast-supported felsic lapilli-crystal tuff, with blue quartz eyes; D) felsic crystal tuff with feldspar fragments and blue quartz eyes; E) amygdaloidal rhyolite; F) aphyric rhyolite; G) quartz-feldspar porphyritic intrusive rock, containing blue quartz and feldspar phenocrysts; H) felsic lapilli-crystal tuff with blue quartz eyes; I) tuffaceous argillite with lapilli. Abbreviations: Arg = argillite, fsp = feldspar, qtz = quartz.

local laminae that signify $S_0$ bedding planes (Fig. 10C). Second, primary features are recognized in volcaniclastic rocks despite vertical compressional strain (i.e., flattening), such as lapilli and crystal fragments that are variably oriented with the $S_1$ fabric (Figs. 9–11). Bradshaw et al. (2008) note that stratigraphy in the vicinity of the Wolverine deposit is deformed and significantly flattened, but primary stratigraphic and deposit morphologies can still be deciphered. This indicates that although the rocks are metamorphosed to phyllite and schist, conditions were not conducive to full recrystallization and fold-induced thickening of the strata in the study areas. Third, although folding of early penetrative foliation is relatively common throughout the Wolverine Lake group, we interpret the footwall stratigraphy to be situated on the eastern limb of an open N-NE–trending anticline that was not affected by intense strain of a hinge region (e.g., Murphy and Piercey, 1999). Strain intensity increases above the Wolverine Lake group hanging wall in the overlying Money Creek (YTT)

and Campbell Range formations (SMT); however, folding is interpreted to not impact the stratigraphic thickness of the Wolverine Lake group footwall stratigraphy (Figs. 5, 7; Murphy and Piercey, 1999; Murphy et al., 2006). Furthermore, we are confident that thickness estimates are reasonable despite widespread strain.

In light of the above points, cross sections were constructed in orientations that are roughly orthogonal to the strike of the penetrative foliation in each area ($S_{1-GLg}$ and $S_{1-WLg}$; Figs. 4–7). For the Kudz Ze Kayah formation, Late Devonian porphyritic granites of the Grass Lakes plutonic suite intrude the entire Grass Lakes group and are thus omitted from thickness reconstructions (Figs. 1, 3, 4). On the surface, these porphyritic rocks are ~40- to 60-m-thick sills in the middle part of the Kudz Ze Kayah formation, whereas units in the western Kudz Ze Kayah formation are thicker (~200–250 m; Fig. 4). In the Wolverine Lake group, porphyritic rocks are interpreted as synvolcanic intrusive rocks (e.g., Piercey et al., 2008),
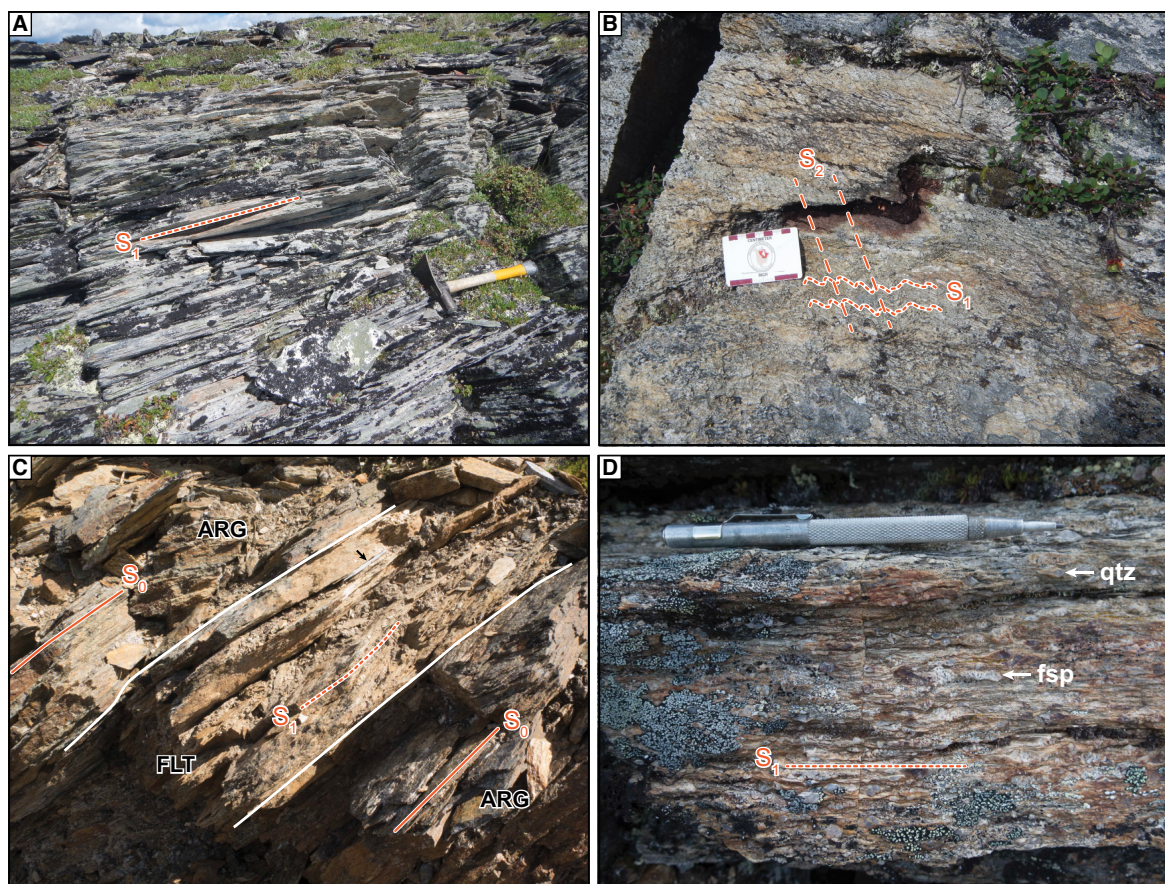
Fig. 10. Representative structural fabrics in the Kudz Ze Kayah formation (A-B) and the Wolverine Lake group footwall (C-D). Pervasive $S_1$ cleavage is the dominant planar feature in both geologic units. A) Prominent $S_1$ cleavage in an outcrop of felsic tuff, with a broadly west-east strike that dips to the north. B) Crenulation fabrics in a felsic tuff developed on an earlier $S_1$ cleavage, with a $S_2$ cleavage superimposed highly oblique to $S_1$. C) Intercalated argillite (ARG) and felsic tuff (FLT) in the upper Wolverine Lake group footwall. Laminations of argillite beds represent primary bedding ($S_0$), and $S_1$ cleavage in the FLT unit is subparallel to bedding. D) Quartz-feldspar porphyritic intrusive rock with strong mineral alignment subparallel to the prominent $S_1$ cleavage.

confirmed by U-Pb dating (below), and included in thickness measurements. Large-scale folds are taken into account in the Wolverine Lake group, and thicknesses are calculated based on the open fold patterns (Fig. 7). Cross sections in the Kudz Ze Kayah formation cross the high-angle East and Fault Creek faults ($D_4$) and are corrected for a maximum of ~320 m of normal displacement; the $D_4$ faults in the Wolverine Lake group, however, are roughly parallel to and therefore do not intersect the cross sections. To avoid assumptions related to the intensity of strain throughout the study areas, the degree of compression is left uncorrected, and the final thicknesses and associated rates presented are thus minimum estimates. Finally, due to the lack of high-precision geochronological constraints above the Kudz Ze Kayah formation and Wolverine Lake group, the Wind Lake formation and Wolverine Lake group hanging-wall strata, respectively, are not included in rate calculations below.

## Previous Geochronology Results

Previous geochronology studies in the Finlayson Lake district have primarily focused on defining the relationship of stratigraphic horizons to a broad tectonostratigraphic framework of the Yukon-Tanana terrane (Mortensen, 1983, 1992; Grant, 1997; Piercey, 2001; Devine et al., 2006; Murphy et al., 2006; Piercey et al., 2008). In the vicinity of the Kudz Ze Kayah and Wolverine VMS deposits, there are 14 historic U-Pb dates that were completed using air-abrasion pretreatment techniques on multigrain fractions (Fig. 3). These dates broadly define limits on the upper Fire Lake formation (ca. 366–365 Ma; $n$ = 2), Grass Lakes plutonic suite (ca. 362–357 Ma; $n$ = 3), and Wolverine Lake group (ca. 356–346 Ma; $n$ = 7). Dates available for the Kudz Ze Kayah formation (ca. 357–347 Ma; $n$ = 3) and the Wolverine Lake group hanging wall (ca. 360 Ma; $n$ = 1) are of poor quality (e.g., contain components of Pb-loss and inheritance) and no longer fit with updated stratigraphic constraints (Murphy et al., 2006). Two periods of magmatism in the upper footwall of the Wolverine Lake group have been defined by porphyritic rocks associated with VMS mineralization at 1) ca. 352 Ma: pre-VMS quartz-feldspar porphyritic intrusions (Sable zone: 352.4 ± 1.5 Ma; Puck zone: 356.9 ± 0.5 Ma); and 2) ca. 347 Ma: syn- to post-VMS feldspar porphyritic intrusions (Wolverine/Lynx zone: 347.8 ± 1.3 Ma; Fisher zone: 346.0 ± 2.2 Ma; Piercey et al., 2008).
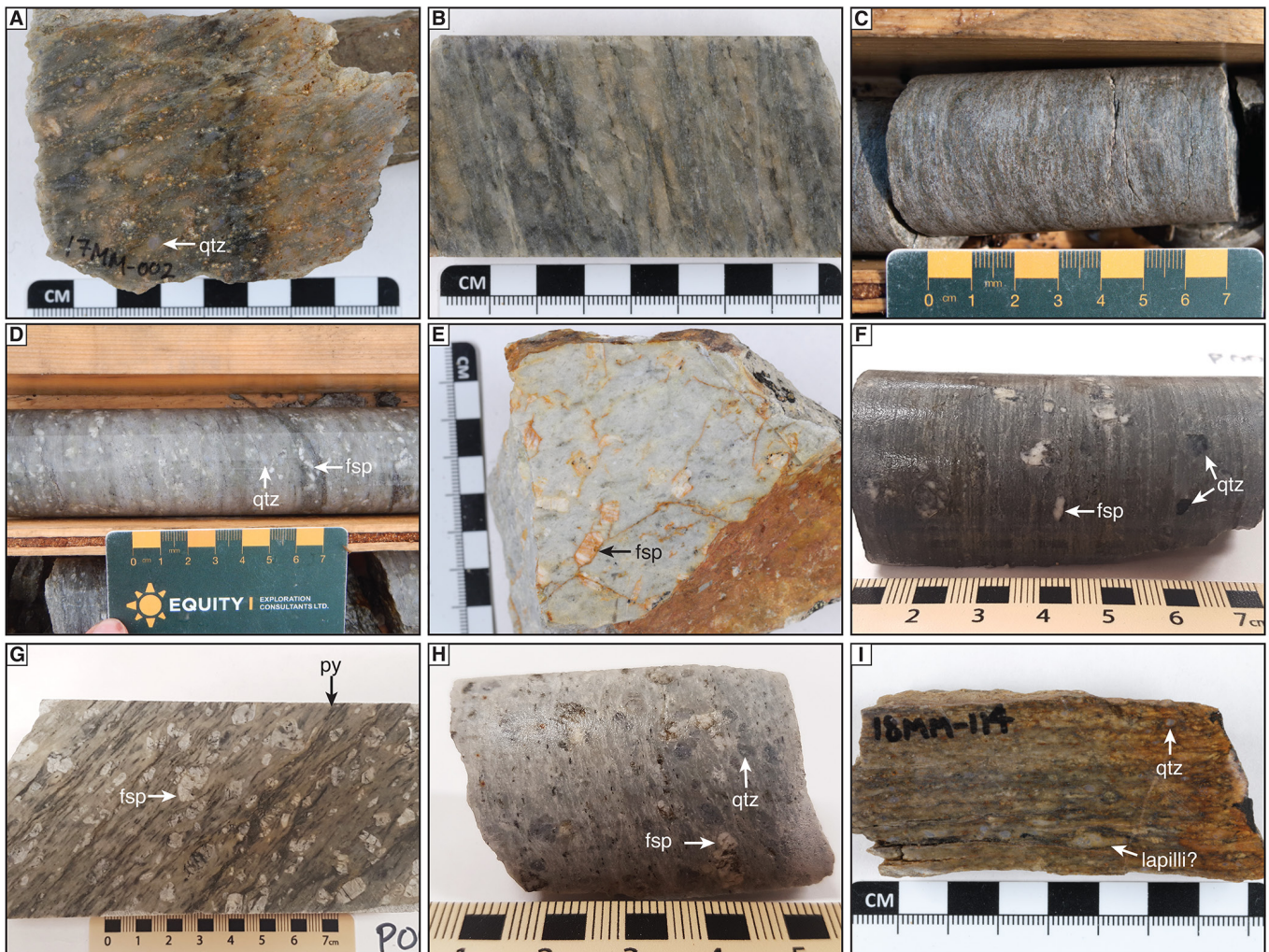
Fig. 11. Rock samples used for chemical abrasion-isotope dilution-thermal ionization mass spectrometery (CA-ID-TIMS) U-Pb zircon geochronology in the Kudz Ze Kayah formation (A-D) and the Wolverine Lake group (E-I). A) Felsic crystal tuff with blue quartz eyes located ~5 m below the Wind Lake-Kudz Ze Kayah formation contact (17MM-002). B) Felsic tuff to lapilli tuff in the hanging wall of the ABM zone (17MM-031). C) Felsic tuff with minor lapilli in the footwall of the Krakatoa horizon (18MM-133). D) Felsic crystal tuff with feldspar and blue quartz in the footwall of the GP4F deposit (17MM-074). E) Feldspar porphyritic intrusive rock in the Fisher zone (18MM-102). F) Felsic crystal tuff with feldspar and quartz fragments from the footwall of the Wolverine/Lynx zone (P99-WV-4K). G) Feldspar porphyritic intrusive rock from the footwall of the Wolverine/Lynx zone (P00-WV-1C). H) Quartz-feldspar porphyritic intrusive rock from the Sable zone (P00-WV-12). I) Felsic crystal tuff with quartz and feldspar in the lower Wolverine Lake group footwall (18MM-114). Mineral abbreviations: fsp = feldspar, py = pyrite, qtz = quartz.

## Analytical Methods

Sample preparation and mineral separation procedures were carried out at Memorial University of Newfoundland (MUN). Zircon was extracted from rock samples following a series of crushing, grinding, splitting, sieving (to <500 µm to >63 µm), heavy liquid (bromoform, methylene iodide), and magnetic separation methods. The zircon grains were then hand-picked in ethanol, loaded into quartz crucibles, and placed into a furnace for annealing at 900°C for 60 hours to treat minor radiation damage; annealing enhances cathodoluminescence (CL) emission (Nasdala et al., 2002), promotes more reproducible interelement fractionation during laser ablation-inductively coupled plasma-mass spectrometry (LA-ICP-MS; Allen and Campbell, 2012), and prepares the crystals for subsequent chemical abrasion (Mattinson, 2005). Annealed grains were mounted in epoxy and ground and polished with 12-µm Al oxide grit, 3-µm diamond paper, and 1-µm Al oxide powder in steps until the grains were sectioned approximately halfway through. Samples were then carbon coated and imaged with cathodoluminscence (CL), backscattered electron (BSE), and secondary electron (SE) techniques at voltages of 10kV (CL) and 15kV (BSE, SE) on a JEOL JSM 7100F scanning electron microscope equipped with a Schottky-type Field Emission gun and a Deben Centaurus CL detector. Zircon CL images are presented in Figure 12 and Appendix Figures A3 and A4.

LA-ICP-MS and CA-ID-TIMS analyses were performed at the Isotope Geology Laboratory at Boise State University, Idaho (BSU). The LA-ICP-MS analyses were completed prior to CA-ID-TIMS to target and omit zircon grains with components of Pb loss or inheritance that would otherwise

**A) Kudz Ze Kayah formation**

*17MM-002* — z6, z7

*17MM-031* — z6, z5

*18MM-133* — z7, z4

*17MM-074* — z2, z8

**B) Wolverine Lake group footwall**

*18MM-102* — z1, z5

*P99-WV-4K* — z1, z3

*P00-WV-1C* — z2, z7

*P00-WV-12* — z6, z4
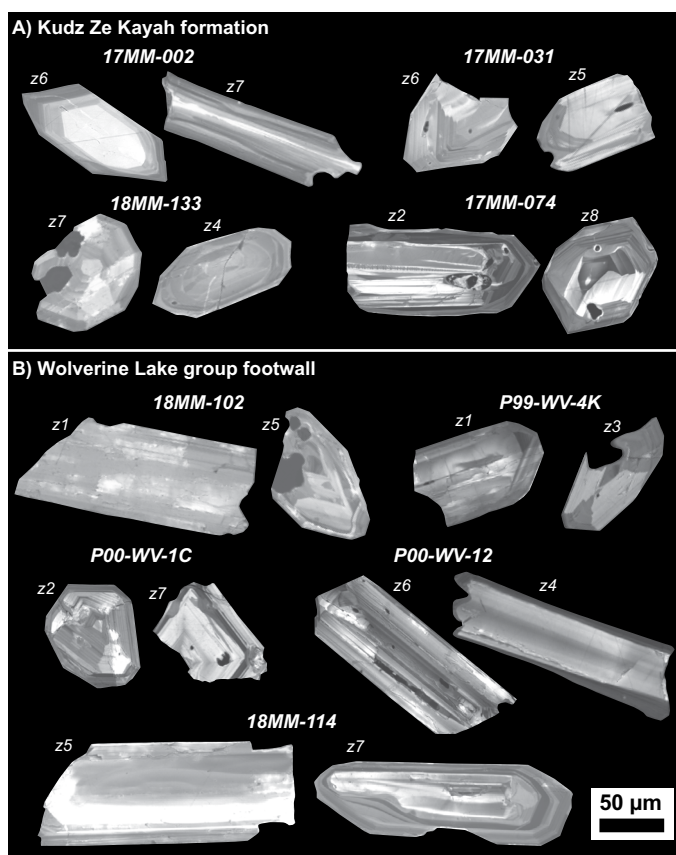
*18MM-114* — z5, z7

50 µm

Fig. 12. Representative cathodoluminescence images for zircon selected for chemical abrasion-isotope dilution-thermal ionization mass spectrometer (CA-ID-TIMS) analysis in A) the Kudz Ze Kayah formation and B) the Wolverine Lake group footwall. Each grain corresponds to an individual CA-ID-TIMS analysis that corresponds with Table 1. The 50-micron scale bar is applicable to all grains in the figure.

The results for LA-ICP-MS U-Pb analysis on zircon standards show concordant $^{206}Pb/^{238}U$ dates of 337.02 ± 0.50 Ma for Plešovice ($2\sigma$; $n$ = 245; mean square of weighted deviates [MSWD] = 1.00), 527.1 ± 1.8 Ma for Seiland ($2\sigma$; $n$ = 125; MSWD = 1.2), and 326.87 ± 0.91 Ma for Zirconia ($2\sigma$; $n$ = 128; MSWD = 1.9; App. Fig. A5). The U-Pb dates are consistent with published $^{206}Pb/^{238}U$ dates for Plešovice (337.13 ± 0.37 Ma; Sláma et al., 2008), Seiland (531 ± 2 Ma; Pedersen et al., 1989), and Zirconia (327.24 ± 0.048 Ma; Boise State University in-house standard) zircon standards.

CA-ID-TIMS U-Pb geochronology methods for isotope dilution thermal ionization mass spectrometry follow those previously published by Davydov et al. (2010) and Schmitz and Davydov (2012). Zircon crystals were plucked from the epoxy mount following LA-ICP-MS analysis and subjected to a modified version of the chemical abrasion method of Mattinson (2005), whereby single crystal fragments plucked from grain mounts were individually abraded in a single step with concentrated HF at 190°C for 12 h. The CA treatment effectively eliminates zircon domains that have experienced post-crystallization Pb loss, thereby producing more concordant and accurate U-Pb dates. Zircon fragments were dissolved in Parr bombs at 220°C for 48 h. Dissolved zircon solutions were subsequently dried down, redissolved in 100 µl of 6N HCl and converted to chlorides in Parr bombs at 180°C for 12 h, after which solutions were dried again and brought up in 50 µl of 3N HCl. Uranium and Pb were isolated by anion exchange column chromatography using 50-µl columns and AG-1 X8 resin (200–400 mesh, chloride form [Eichrom]; Krogh, 1973).

The U-Pb aliquot was loaded in a silica gel emitter (Gerstenberger and Haase, 1997) to an outgassed, zone-refined Re filament. Isotopic determinations were performed using an IsotopX PhoeniX-62 TIMS. A correction for mass-dependent Pb fractionation was applied based on repeated measurements of NBS 982 (Catanzaro et al., 1968) Pb (on both the Daly ion counter [0.16 ± 0.03 %] amu$^{-1}$; 1$s$) and the Faraday cups (0.10 × [1 ± 0.02%] amu$^{-1}$; 1$s$). Uranium was run as an oxide (UO$_2$) and measured in static mode on Faraday detectors equipped with 10$^{12}$ Ω resistors. The U mass fractionation for the same analyses was calculated using the $^{233}U/^{235}U$ ratio of the EARTHTIME ET535 mixed $^{233-235}U-^{205}Pb$ double spike solution (0.99506 ± 0.01%, 1$s$). The EARTHTIME ET2535 mixed $^{233-235}U-^{202-205}Pb$ double spike solution (0.99923 ± 0.027%, 1$s$) was also utilized for certain samples (denoted by * beside the sample number in Table 1) and, where applicable, the mass-dependent Pb fractionation was corrected for during the run.

Raw U and Pb data were filtered using the Tripoli software program (Bowring et al., 2011), and the U-Pb dates and uncertainties for each analysis were calculated using the algorithms of Schmitz and Schoene (2007), the U decay constants of Jaffey et al. (1971), and a value of $^{238}U/^{235}U$ = 137.88. Uranium oxide measurements were corrected for isobaric interferences using an $^{18}O/^{16}O$ value of 0.00206. Uncertainties are based upon non-systematic analytical errors, including counting statistics, instrumental fractionation, tracer subtraction, and blank subtraction. All non-radiogenic Pb was attributed to laboratory blank with a mean isotopic composition determined by total procedural blank measurements. These error estimates should be considered when comparing the $^{206}Pb/^{238}U$ dates

be unsuitable for obtaining high-precision CA-ID-TIMS analyses. Laser ablation was performed on each grain using a New Wave Research UP-213 Nd:YAG UV laser (213 nm) using fluence and pulse rates of ~5 J/cm$^2$ and 10 Hz, respectively, during a 45-second analysis (15-sec gas blank, 30-sec ablation). Spot sizes are 25 µm in diameter and, where necessary, raster lines of 10-µm diameter and ~50-mm length were used to avoid burning through grains. Ablated material was carried by a 1.2-L/min He gas stream to the nebulizer flow of the plasma and analyzed in a ThermoElectron X-Series II quadrupole ICP-MS. Quadrupole dwell times were 5 ms for Si and Zr, 200 ms for $^{49}Ti$ and $^{207}Pb$, 80 ms for $^{206}Pb$, 40 ms for $^{202}Hg$, $^{204}Pb$, $^{208}Pb$, $^{232}Th$, and $^{238}U$, and 10 ms for all other high field strength elements (HFSEs) and rare earth elements (REEs); total sweep duration is 950 ms. Background count rates for each analyte were obtained prior to each spot analysis and subtracted from the raw count rate for each analyte. For concentration calculations, background-subtracted count rates for each analyte were internally normalized to $^{29}Si$ and calibrated with respect to NIST SRM-610 and -612 glasses as the primary standards. Standards (Plešovice, Seiland, and Zirconia) were used throughout the run, four for every ten unknowns, to monitor for instrument drift. Data processing was completed with a BSU in-house Excel-based program.

with those from other laboratories that used tracer solutions calibrated against the EARTHTIME gravimetric standards. When comparing our dates with those derived from other isotopic decay schemes (e.g., $^{40}Ar/^{39}Ar$, $^{187}Re$-$^{187}Os$), the uncertainties in tracer calibration (0.05%; Condon et al., 2015; McLean et al., 2015) and U decay constants (0.108%; Jaffey et al., 1971) should be added to the internal error in quadrature. Quoted errors for calculated weighted means are thus of the form $\pm X/Y/Z$ ($\pm 2\sigma$), where X is solely analytical uncertainty, Y is the combined analytical and tracer uncertainty, and Z is the combined analytical, tracer and $^{238}U$ decay constant uncertainty (Schoene et al., 2006). Concordia diagrams, regression intercepts, and weighted averages were produced with Isoplot 4.1 (Ludwig, 2003). Results are presented as $^{206}Pb/^{238}U$ isotope ratios for all of the CA-ID-TIMS and LA-ICP-MS samples <1 Ga; those grains with dates >1 Ga are reported in the text as $^{207}Pb/^{206}Pb$ dates. Unless otherwise noted, grains with young LA-ICP-MS dates that are not included in the weighted mean are interpreted to reflect post-crystallization Pb loss. The CA-ID-TIMS results are reported in Table 1 and Figures 13 and 14; LA-ICP-MS results are presented in Appendix Tables A1 and A2, and Figures A5 and A6.

## CA-ID-TIMS and LA-ICP-MS U-Pb Zircon Geochronology

Integrated field mapping and drill core logging were utilized for precise stratigraphic sampling in the Upper Devonian Kudz Ze Kayah formation and the Early Mississippian Wolverine Lake group (Figs. 3–5). Four CA-ID-TIMS samples were collected in the Kudz Ze Kayah formation, and five samples were obtained from the Wolverine Lake group for the purpose of precisely defining the ages of important VMS deposits in the Finlayson Lake district (i.e., Kudz Ze Kayah, GP4F, and Wolverine) and constraining ages of host stratigraphy in each rock package (Fig. 11). Detailed rock descriptions are presented in the Appendix.

### Reporting of CA-ID-TIMS U-Pb zircon dates

The dispersion of individual CA-ID-TIMS $^{206}Pb/^{238}U$ dates indicates that protracted crystallization of zircon occurred during the formation of rocks in the Finlayson Lake district (Table 1; Figs. 12, 13). Protracted crystallization suggests that the oldest zircon date represents the time of zircon saturation, whereas the youngest date represents the final stage of zircon crystallization at the solidus temperature (e.g., Wotzlaw et al., 2013; Rioux et al., 2012; Samperton et al., 2015); the established array is thus defined by a total duration ($\Delta t$) of zircon within the host magma that includes the $2\sigma$ uncertainty (95% confidence interval). However, for each individual sample presented for the Kudz Ze Kayah formation and Wolverine Lake group, the individual zircon dates record uncertainties that are in many cases larger than the dispersion between each zircon date (e.g., Fig. 13). Therefore, we report a single weighted mean $^{206}Pb/^{238}U$ date for each sample population with a $2\sigma$ uncertainty that directly overlaps within error of the youngest individual zircon date.

### Kudz Ze Kayah formation

*Kudz Ze Kayah-Wind Lake formation contact (17MM-002):* Sample 17MM-002 yielded zircon that is euhedral and elon-

gate ranging from 120 to 200 $\mu$m with high aspect ratios (~3:1 to 5:1). The grains typically have oscillatory zoning with the brightest CL response near the core of the grains (Fig. 12A, App. Fig. A3). The CA-ID-TIMS analytical results for seven individual fractions are concordant, contain relatively low Th/U (0.16–0.54), and yield a weighted mean $^{206}Pb/^{238}U$ date of 362.404 ± 0.098 Ma ($2\sigma$; MSWD = 0.55; Table 1; Fig. 13A). Fraction z5 is interpreted as a xenocryst due to its higher Th/U (0.86) and a concordant U-Pb date of ~363.4 Ma. The LA-ICP-MS results gave concordant Th/U (0.13–2.2) and a weighted mean $^{206}Pb/^{238}U$ date of 365.1 ± 2.7 Ma ($2\sigma$; MSWD = 1.6; $n$ = 35) that overlaps within error of the CA-ID-TIMS date. Four zircon grains gave older dates between ca. 378 to 397 Ma ($n$ = 3) and ca. 1720 Ma ($n$ = 1), which are all interpreted as xenocrysts.

*ABM hanging wall (17MM-031):* Zircon grains from this sample (17MM-031) are euhedral and typically 80 to 120 $\mu$m (aspect ratio 1:1 to ~2:1); rare grains are >200 $\mu$m and have high aspect ratios (~5:1). The zircon grains have oscillatory CL-bright to CL-dark zones with minor CL-bright sector zones (e.g., z7; Fig. 12A, App. Fig. A3). The CA-ID-TIMS data gave seven concordant fractions with high Th/U (0.67 and 1.01–1.15) and a weighted mean $^{206}Pb/^{238}U$ date of 362.82 ± 0.12 Ma ($2\sigma$; MSWD = 0.84; Table 1; Fig. 13B), inferred as the timing of eruption and approximate age of the ABM deposit (Fig. 2C). The LA-ICP-MS analytical results are concordant with variable Th/U (0.15–1.8) and a weighted mean $^{206}Pb/^{238}U$ date of 361.2 ± 2.4 Ma ($2\sigma$; MSWD = 0.55; $n$ = 32); this date overlaps the CA-ID-TIMS date within error. One grain yielded an older $^{207}Pb/^{206}Pb$ date of ca. 2350 Ma and is interpreted as a xenocryst.

*Krakatoa footwall (18MM-133):* Zircon grains from sample 18MM-133 are euhedral and ~80 to 120 $\mu$m in length with aspect ratios near ~2:1. The grains have oscillatory zoning with alternating CL-bright and CL-dark zones, and minor sector zoning (Fig. 12A, App. Fig. A3). The CA-ID-TIMS results show seven concordant zircon fractions with high Th/U (0.99–1.2, $n$ = 6), where one fraction yielded a low Th/U of 0.20 (z5). These seven grains gave a weighted mean $^{206}Pb/^{238}U$ date of 362.847 ± 0.099 Ma ($2\sigma$; MSWD = 0.47; Table 1; Fig. 13C), which is equivalent within uncertainty to the ABM hanging wall (17MM-031); this date is interpreted as the eruption age of this rock and approximate age of the Krakatoa deposit. One zircon fraction (z10) overlaps with the weighted mean U-Pb date but is not included in the weighted mean calculation because of its high uncertainty that increases the MSWD. The LA-ICP-MS results are concordant with variable Th/U (0.42–3.8) and a weighted mean $^{206}Pb/^{238}U$ date of 360.0 ± 1.6 Ma ($2\sigma$; MSWD = 0.70; $n$ = 34), which is younger outside of $2\sigma$ uncertainty than the CA-ID-TIMS date. One grain gave an older $^{207}Pb/^{206}Pb$ date of ca. 1130 Ma and is interpreted as a xenocryst.

*GP4F footwall (17MM-074):* Zircon grains in this rock are euhedral, with rare subhedral dipyramid terminations, and vary in length (~75–120 $\mu$m) and aspect ratio (1:1 to 3:1; Fig. 12A, App. Fig. A3). The zircon grains typically display oscillatory zoning with CL-bright cores and relatively CL-dark rims, with rare CL-bright sector zones (e.g., z8). The CA-ID-TIMS data yields eight concordant zircon fractions with variable Th/U; five fractions have Th/U between 0.27 and 0.47, while three have higher Th/U (0.83–1.2). The weighted
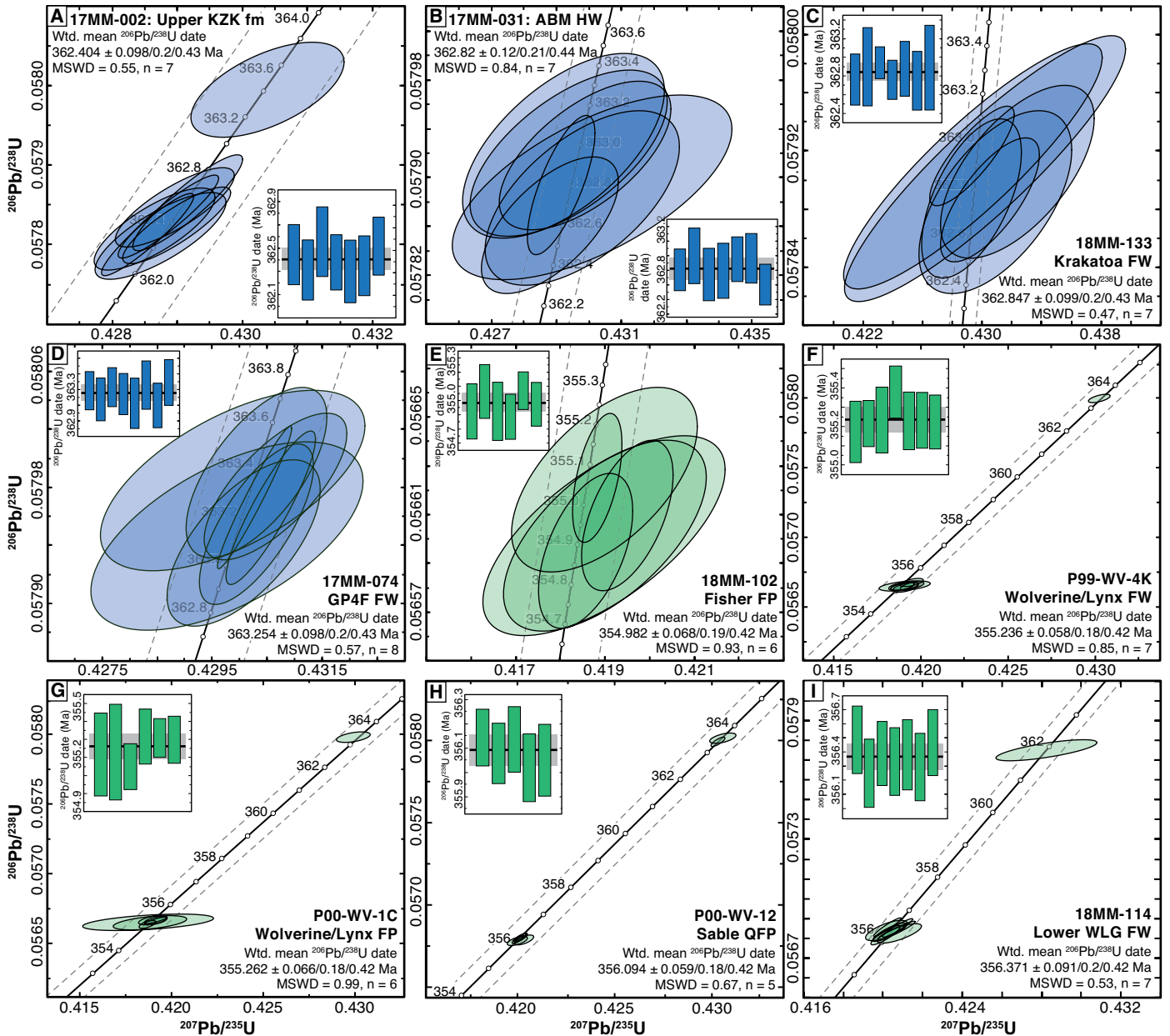
Fig. 13. Concordia diagrams showing chemical abrasion-isotope dilution-thermal ionization mass spectrometry (CA-ID-TIMS) U-Pb geochronology results for zircon in rocks from the Kudz Ze Kayah formation (A-D) and the Wolverine Lake group (E-I). A) Felsic crystal tuff at the Kudz Ze Kayah-Wind Lake formation contact (17MM-002); B) felsic lapilli tuff in the ABM hanging wall (17MM-031); C) felsic tuff from the Krakatoa footwall (18MM-133); D) felsic crystal tuff in the GP4F footwall (17MM-074); E) feldspar-porphyritic rhyolite from the Fisher zone (FP; 18MM-102); F) felsic tuff in the Wolverine/Lynx footwall (P99-WV-4K); G) feldspar-porphyritic rhyolite from the Wolverine/Lynx zone (P00-WV-1C); H) quartz-feldspar-porphyritic rhyolite from the Sable zone (QFP; P00-WV-12); and I) felsic crystal tuff from the lower Wolverine Lake group footwall (18MM-114). Each individual ellipse encompasses the $2\sigma$ error on a single zircon analytical result. The gray dashed lines represent the range of decay constant uncertainty on the concordia curve. The inset panels show individual grain analyses with their included $2\sigma$ error (vertical bars); the solid black line indicates the calculated weighted mean $^{206}Pb/^{238}U$ date, and the larger gray region indicates the error associated with external reproducibility of the analyses. Ellipse and bar colors correspond to the ranked bars in Fig. 14. Abbreviations: FW = footwall, HW = hanging wall, MSWD = mean square of weighted deviates, Wtd. = weighted.

mean $^{206}Pb/^{238}U$ date for this zircon population is 363.254 ± 0.098 Ma ($2\sigma$; MSWD = 0.57; Table 1; Fig. 13D), interpreted to be the eruption age of this rock, the approximate age of the GP4F deposit, and the oldest date in the Kudz Ze Kayah formation. The LA-ICP-MS data is concordant with a range

of Th/U (0.13–4.3) and a weighted mean $^{206}Pb/^{238}U$ date of 363.1 ± 2.3 Ma ($2\sigma$; MSWD = 0.67; $n$ = 40); this date is within uncertainty of the CA-ID-TIMS date. Two grains have older dates of ca. 383 and 1770 Ma, which are both interpreted as xenocrystic zircon.

Table 1. Chemical Abrasion-ID-TIMS U-Pb Zircon Geochronology Results for Rocks in the Kudz Ze Kayah Formation and Wolverine Lake Group, Finlayson Lake District, Yukon

| Sample[1] | U (ppm) | Th (ppm) | Th/U[2] | $^{206}Pb^*$ x10$^{-13}$mol[3] | mol% $^{206}Pb^*$[3] | Pb*/Pbc | Pbc (pg)[3] | $\frac{^{206}Pb}{^{204}Pb}$[4] | $\frac{^{208}Pb}{^{206}Pb}$[5] | $\frac{^{207}Pb}{^{206}Pb}$[5] | % err[6] | $\frac{^{207}Pb}{^{235}U}$[5] | % err[6] | $\frac{^{206}Pb}{^{238}U}$[5] | % err[6] | corr. coef. | $\frac{^{207}Pb}{^{206}Pb}$[7] | ±[6] | $\frac{^{207}Pb}{^{235}U}$[7] | ±[6] | $\frac{^{206}Pb}{^{238}U}$[7] | ±[6] |
|---|---|---|---|---|---|---|---|---|---|---|---|---|---|---|---|---|---|---|---|---|---|---|
| **Kudz Ze Kayah formation** | | | | | | | | | | | | | | | | | | | | | | |
| **1) 17MM-074 – felsic crystal tuff (GP4F footwall; 419498 E, 6813353 N)** | | | | | | | | | | | | | | | | | | | | | | |
| z1 | 654 | 246 | 0.376 | 15.8017 | 99.93% | 424 | 0.90 | 26246 | 0.119 | 0.05383 | 0.063 | 0.430263 | 0.127 | 0.057973 | 0.069 | 0.967 | 363.85 | 1.4 | 363.36 | 0.39 | 363.29 | 0.24 |
| z2 | 44 | 21 | 0.467 | 1.0721 | 99.58% | 71 | 0.38 | 4283 | 0.147 | 0.05385 | 0.151 | 0.430302 | 0.197 | 0.057954 | 0.078 | 0.724 | 364.78 | 3.4 | 363.39 | 0.60 | 363.17 | 0.28 |
| z3 | 52 | 14 | 0.274 | 1.2521 | 99.10% | 31 | 0.94 | 2012 | 0.086 | 0.05387 | 0.200 | 0.430654 | 0.245 | 0.057980 | 0.071 | 0.720 | 365.61 | 4.5 | 363.64 | 0.75 | 363.33 | 0.25 |
| z4 | 39 | 32 | 0.825 | 0.9382 | 99.66% | 96 | 0.26 | 5324 | 0.260 | 0.05387 | 0.093 | 0.430569 | 0.154 | 0.057966 | 0.075 | 0.895 | 365.73 | 2.1 | 363.58 | 0.47 | 363.24 | 0.26 |
| z5 | 7 | 8 | 1.202 | 0.1683 | 98.53% | 24 | 0.21 | 1227 | 0.379 | 0.05379 | 0.423 | 0.429767 | 0.470 | 0.057946 | 0.091 | 0.584 | 362.30 | 9.5 | 363.01 | 1.43 | 363.12 | 0.32 |
| z6 | 11 | 5 | 0.431 | 0.2670 | 98.26% | 17 | 0.39 | 1038 | 0.136 | 0.05377 | 0.408 | 0.429874 | 0.456 | 0.057985 | 0.088 | 0.607 | 361.35 | 9.2 | 363.09 | 1.39 | 363.36 | 0.31 |
| z7 | 20 | 20 | 1.002 | 0.4785 | 99.21% | 43 | 0.32 | 2289 | 0.316 | 0.05383 | 0.220 | 0.430069 | 0.263 | 0.057942 | 0.081 | 0.645 | 364.05 | 5.0 | 363.23 | 0.80 | 363.10 | 0.29 |
| z8 | 19 | 7 | 0.357 | 0.4703 | 99.46% | 53 | 0.21 | 3316 | 0.113 | 0.05382 | 0.199 | 0.430301 | 0.243 | 0.057990 | 0.083 | 0.652 | 363.39 | 4.5 | 363.39 | 0.74 | 363.39 | 0.29 |
| **2) 18MM-133* – felsic tuff (Krakatoa footwall; 415246 E, 6815342 N)** | | | | | | | | | | | | | | | | | | | | | | |
| z1 | 5 | 6 | 1.264 | 0.1204 | 97.89% | 4 | 0.22 | 854 | 0.398 | 0.05379 | 0.597 | 0.429305 | 0.639 | 0.057887 | 0.078 | 0.581 | 362.17 | 13.5 | 362.68 | 1.95 | 362.76 | 0.27 |
| z2 | 12 | 12 | 0.990 | 0.2918 | 92.81% | 4 | 1.88 | 251 | 0.312 | 0.05378 | 1.554 | 0.429391 | 1.658 | 0.057910 | 0.119 | 0.888 | 361.75 | 35.0 | 362.74 | 5.06 | 362.90 | 0.42 |
| z3 | 8 | 9 | 1.186 | 0.1933 | 98.31% | 21 | 0.28 | 1070 | 0.374 | 0.05376 | 0.506 | 0.429326 | 0.546 | 0.057916 | 0.048 | 0.833 | 361.14 | 11.4 | 362.70 | 1.66 | 362.94 | 0.17 |
| z4 | 19 | 4 | 0.197 | 0.4594 | 97.29% | 10 | 1.06 | 666 | 0.062 | 0.05394 | 0.588 | 0.430527 | 0.629 | 0.057886 | 0.060 | 0.723 | 368.60 | 13.2 | 363.55 | 1.92 | 362.76 | 0.21 |
| z5 | 4 | 4 | 1.071 | 0.0922 | 97.83% | 16 | 0.17 | 831 | 0.337 | 0.05416 | 0.922 | 0.432382 | 0.971 | 0.057906 | 0.084 | 0.616 | 377.54 | 20.7 | 364.87 | 2.98 | 362.88 | 0.30 |
| z6 | 3 | 4 | 1.131 | 0.0804 | 96.43% | 9 | 0.25 | 505 | 0.357 | 0.05399 | 0.929 | 0.430891 | 0.976 | 0.057885 | 0.089 | 0.571 | 370.58 | 20.9 | 363.81 | 2.99 | 362.75 | 0.31 |
| z8 | 6 | 7 | 1.086 | 0.1487 | 92.37% | 4 | 1.02 | 237 | 0.342 | 0.05388 | 1.678 | 0.430206 | 1.793 | 0.057908 | 0.129 | 0.900 | 366.09 | 37.8 | 363.32 | 5.48 | 362.89 | 0.45 |
| z10 | 1 | 1 | 1.167 | 0.0262 | 86.76% | 2 | 0.33 | 136 | 0.368 | 0.05388 | 5.660 | 0.429600 | 5.841 | 0.057833 | 0.409 | 0.470 | 365.84 | 127.6 | 362.89 | 17.82 | 362.43 | 1.44 |
| **3) 17MM-031 – felsic tuff (ABM hanging wall; 415050 E, 6815465 N)** | | | | | | | | | | | | | | | | | | | | | | |
| z1 | 52 | 53 | 1.015 | 1.2594 | 99.74% | 132 | 0.27 | 6993 | 0.320 | 0.05376 | 0.147 | 0.429151 | 0.197 | 0.057894 | 0.081 | 0.744 | 361.10 | 3.3 | 362.57 | 0.60 | 362.80 | 0.28 |
| z2 | 10 | 6 | 0.669 | 0.2327 | 97.91% | 15 | 0.41 | 864 | 0.211 | 0.05374 | 0.533 | 0.429208 | 0.590 | 0.057926 | 0.107 | 0.598 | 360.15 | 12.0 | 362.61 | 1.80 | 363.00 | 0.38 |
| z3 | 7 | 8 | 1.067 | 0.1773 | 98.27% | 20 | 0.26 | 1040 | 0.336 | 0.05385 | 0.514 | 0.429788 | 0.567 | 0.057883 | 0.101 | 0.588 | 364.85 | 11.6 | 363.03 | 1.73 | 362.74 | 0.36 |
| z5 | 6 | 7 | 1.152 | 0.1424 | 97.53% | 14 | 0.30 | 731 | 0.363 | 0.05388 | 0.755 | 0.430099 | 0.818 | 0.057892 | 0.107 | 0.631 | 366.15 | 17.0 | 363.25 | 2.50 | 362.79 | 0.38 |
| z6 | 9 | 9 | 1.011 | 0.2266 | 98.06% | 17 | 0.37 | 928 | 0.319 | 0.05383 | 0.452 | 0.429876 | 0.501 | 0.057918 | 0.086 | 0.626 | 363.97 | 10.2 | 363.09 | 1.53 | 362.95 | 0.30 |
| z7 | 5 | 6 | 1.043 | 0.1284 | 97.99% | 17 | 0.22 | 899 | 0.329 | 0.05377 | 0.523 | 0.429384 | 0.577 | 0.057920 | 0.096 | 0.620 | 361.29 | 11.8 | 362.74 | 1.76 | 362.97 | 0.34 |
| z8 | 16 | 18 | 1.143 | 0.3882 | 98.52% | 23 | 0.48 | 1218 | 0.360 | 0.05375 | 0.358 | 0.428799 | 0.403 | 0.057861 | 0.079 | 0.634 | 360.53 | 8.1 | 362.32 | 1.23 | 362.60 | 0.28 |
| **4) 17MM-002 – felsic lapilli tuff (Kudz Ze Kayah fm–Wind Lake fm contact; 413907 E, 6815182 N)** | | | | | | | | | | | | | | | | | | | | | | |
| z1 | 77 | 34 | 0.446 | 1.8587 | 99.81% | 155 | 0.30 | 9439 | 0.140 | 0.05378 | 0.084 | 0.428859 | 0.147 | 0.057835 | 0.074 | 0.923 | 361.86 | 1.9 | 362.37 | 0.45 | 362.44 | 0.26 |
| z2 | 370 | 111 | 0.301 | 8.9212 | 99.89% | 264 | 0.80 | 16681 | 0.095 | 0.05376 | 0.073 | 0.428548 | 0.135 | 0.057813 | 0.073 | 0.929 | 361.08 | 1.6 | 362.14 | 0.41 | 362.31 | 0.26 |
| z3 | 43 | 17 | 0.394 | 1.0350 | 99.65% | 84 | 0.30 | 5180 | 0.124 | 0.05380 | 0.090 | 0.429159 | 0.160 | 0.057853 | 0.085 | 0.905 | 362.74 | 2.0 | 362.58 | 0.49 | 362.55 | 0.30 |
| z4 | 73 | 33 | 0.456 | 1.7683 | 99.76% | 124 | 0.35 | 7527 | 0.144 | 0.05381 | 0.107 | 0.428992 | 0.158 | 0.057824 | 0.068 | 0.855 | 362.99 | 2.4 | 362.46 | 0.48 | 362.38 | 0.24 |
| z5 | 39 | 33 | 0.859 | 0.9320 | 99.70% | 110 | 0.23 | 6023 | 0.271 | 0.05382 | 0.187 | 0.430391 | 0.223 | 0.057994 | 0.084 | 0.583 | 363.69 | 4.2 | 363.45 | 0.68 | 363.42 | 0.30 |
| z6 | 22 | 10 | 0.455 | 0.5337 | 99.62% | 78 | 0.17 | 4722 | 0.143 | 0.05379 | 0.140 | 0.428741 | 0.191 | 0.057811 | 0.076 | 0.774 | 362.17 | 3.2 | 362.28 | 0.58 | 362.30 | 0.27 |
| z7 | 30 | 16 | 0.536 | 0.7334 | 99.75% | 122 | 0.15 | 7279 | 0.169 | 0.05377 | 0.130 | 0.428649 | 0.178 | 0.057819 | 0.073 | 0.774 | 361.37 | 2.9 | 362.22 | 0.54 | 362.35 | 0.26 |
| z8 | 38 | 6 | 0.161 | 0.9176 | 99.72% | 96 | 0.22 | 6333 | 0.051 | 0.05378 | 0.125 | 0.428960 | 0.175 | 0.057847 | 0.071 | 0.804 | 361.93 | 2.8 | 362.44 | 0.53 | 362.52 | 0.25 |
| **Wolverine Lake group** | | | | | | | | | | | | | | | | | | | | | | |
| **5) 18MM-114 – felsic crystal tuff (lower Wolverine Lake group footwall; 439669 E, 6805499 N)** | | | | | | | | | | | | | | | | | | | | | | |
| z1 | 11 | 3 | 0.243 | 0.2624 | 98.38% | 17 | 0.36 | 1112 | 0.077 | 0.05379 | 0.435 | 0.428262 | 0.486 | 0.057747 | 0.073 | 0.731 | 362.16 | 9.8 | 361.94 | 1.48 | 361.91 | 0.26 |
| z2 | 150 | 41 | 0.276 | 3.5483 | 99.90% | 276 | 0.30 | 17613 | 0.087 | 0.05360 | 0.072 | 0.420227 | 0.135 | 0.056858 | 0.069 | 0.950 | 354.43 | 1.6 | 356.21 | 0.40 | 356.49 | 0.24 |
| z3 | 85 | 23 | 0.270 | 2.0112 | 99.83% | 171 | 0.28 | 10905 | 0.085 | 0.05363 | 0.091 | 0.420132 | 0.146 | 0.056819 | 0.070 | 0.876 | 355.47 | 2.1 | 356.15 | 0.44 | 356.25 | 0.24 |
| z4 | 40 | 11 | 0.280 | 0.9401 | 99.53% | 60 | 0.37 | 3838 | 0.088 | 0.05368 | 0.122 | 0.420693 | 0.182 | 0.056842 | 0.066 | 0.948 | 357.57 | 2.8 | 356.55 | 0.55 | 356.39 | 0.23 |
| z5 | 49 | 13 | 0.256 | 1.1576 | 99.73% | 103 | 0.26 | 6622 | 0.081 | 0.05364 | 0.106 | 0.420320 | 0.160 | 0.056832 | 0.070 | 0.866 | 355.94 | 2.4 | 356.28 | 0.48 | 356.33 | 0.24 |
| z6 | 35 | 12 | 0.351 | 0.8253 | 99.58% | 68 | 0.29 | 4258 | 0.111 | 0.05362 | 0.159 | 0.420185 | 0.202 | 0.056840 | 0.073 | 0.703 | 354.91 | 3.6 | 356.18 | 0.61 | 356.38 | 0.25 |
| z7 | 82 | 28 | 0.343 | 1.9380 | 99.35% | 44 | 1.06 | 2758 | 0.108 | 0.05371 | 0.174 | 0.420835 | 0.220 | 0.056826 | 0.070 | 0.750 | 358.93 | 3.9 | 356.65 | 0.66 | 356.29 | 0.24 |
| z8 | 27 | 21 | 0.797 | 0.6289 | 99.70% | 107 | 0.16 | 5971 | 0.251 | 0.05367 | 0.087 | 0.420725 | 0.148 | 0.056854 | 0.068 | 0.940 | 357.25 | 2.0 | 356.57 | 0.45 | 356.46 | 0.23 |

Table 1. (Cont.)

| Sample[1] | U (ppm) | Th (ppm) | Th/U[2] | 206Pb* x10⁻¹³mol[3] | mol % 206Pb*[3] | Pb*c[3] | Pbc (pg)[3] | 206Pb/204Pb[4] | 208Pb/206Pb[5] | 207Pb/206Pb[5] | 207Pb/235U[5] | % err[6] | 206Pb/238U[5] | % err[6] | corr. coef. | 207Pb/206Pb[7] | ±[6] | 207Pb/235U[7] | ±[6] | 206Pb/238U[7] | ±[6] |
|---|---|---|---|---|---|---|---|---|---|---|---|---|---|---|---|---|---|---|---|---|---|
| | | | | | | **Compositional parameters** | | | | | | | **Radiogenic isotope Ratios** | | | | | | **Isotopic ages** | | |
| **Wolverine Lake group** | | | | | | | | | | | | | | | | | | | | | |
| 6) P00-WV-12* – quartz-feldspar porphyritic rhyolite (Sable zone; 440962 E, 6809971 N) | | | | | | | | | | | | | | | | | | | | | |
| z1 | 147 | 87 | 0.591 | 3.4800 | 99.95% | 657 | 0.14 | 38490 | 0.186 | 0.05365 | 0.420162 | 0.029 | 0.056802 | 0.034 | 0.860 | 356.29 | 0.7 | 356.17 | 0.16 | 356.15 | 0.12 |
| z2 | 99 | 45 | 0.457 | 2.3474 | 99.95% | 568 | 0.10 | 34452 | 0.144 | 0.05364 | 0.420024 | 0.037 | 0.056791 | 0.036 | 0.797 | 355.99 | 0.8 | 356.07 | 0.18 | 356.08 | 0.13 |
| z3 | 43 | 30 | 0.700 | 1.0297 | 99.87% | 247 | 0.11 | 14057 | 0.221 | 0.05365 | 0.420170 | 0.044 | 0.056801 | 0.039 | 0.782 | 356.39 | 1.0 | 356.17 | 0.20 | 356.14 | 0.14 |
| z4 | 32 | 19 | 0.607 | 0.7522 | 99.74% | 117 | 0.17 | 6832 | 0.191 | 0.05365 | 0.419997 | 0.082 | 0.056781 | 0.040 | 0.611 | 356.23 | 1.9 | 356.05 | 0.30 | 356.02 | 0.14 |
| z5 | 33 | 38 | 1.157 | 0.7865 | 99.83% | 211 | 0.11 | 10786 | 0.365 | 0.05382 | 0.430313 | 0.044 | 0.057992 | 0.040 | 0.789 | 363.39 | 1.0 | 363.40 | 0.21 | 363.40 | 0.14 |
| z6 | 20 | 12 | 0.577 | 0.4827 | 99.78% | 142 | 0.09 | 8351 | 0.182 | 0.05369 | 0.420343 | 0.076 | 0.056787 | 0.043 | 0.638 | 357.88 | 1.7 | 356.30 | 0.29 | 356.05 | 0.15 |
| z7 | 20 | 25 | 1.259 | 0.4814 | 99.74% | 137 | 0.11 | 6879 | 0.397 | 0.05383 | 0.430562 | 0.109 | 0.058014 | 0.044 | 0.572 | 363.84 | 2.5 | 363.58 | 0.39 | 363.53 | 0.15 |
| 7) P00-WV-1C* – feldspar porphyritic rhyolite (Wolverine/Lynx deposit; 439618 E, 6811350 N) | | | | | | | | | | | | | | | | | | | | | |
| z1 | 4 | 4 | 0.898 | 0.1050 | 98.94% | 31 | 0.09 | 1701 | 0.283 | 0.05362 | 0.418824 | 0.359 | 0.056648 | 0.074 | 0.512 | 355.20 | 8.1 | 355.21 | 1.17 | 355.21 | 0.25 |
| z2 | 3 | 3 | 1.104 | 0.0731 | 98.41% | 22 | 0.10 | 1134 | 0.348 | 0.05361 | 0.418724 | 0.659 | 0.056651 | 0.085 | 0.486 | 354.74 | 14.9 | 355.14 | 2.08 | 355.23 | 0.29 |
| z3 | 42 | 44 | 1.052 | 0.9911 | 99.82% | 190 | 0.15 | 9973 | 0.332 | 0.05362 | 0.418685 | 0.070 | 0.056636 | 0.041 | 0.629 | 354.95 | 1.6 | 355.11 | 0.26 | 355.14 | 0.14 |
| z4 | 13 | 13 | 0.979 | 0.3030 | 99.66% | 99 | 0.09 | 5267 | 0.309 | 0.05363 | 0.418986 | 0.134 | 0.056666 | 0.048 | 0.539 | 355.36 | 3.0 | 355.33 | 0.46 | 355.32 | 0.17 |
| z5 | 16 | 17 | 1.031 | 0.3804 | 99.68% | 106 | 0.10 | 5604 | 0.325 | 0.05365 | 0.419151 | 0.087 | 0.056665 | 0.034 | 0.873 | 356.31 | 2.0 | 355.44 | 0.35 | 355.31 | 0.12 |
| z6 | 14 | 16 | 1.108 | 0.3452 | 99.55% | 77 | 0.13 | 4022 | 0.349 | 0.05378 | 0.429908 | 0.156 | 0.057979 | 0.053 | 0.491 | 361.77 | 3.5 | 363.11 | 0.53 | 363.32 | 0.19 |
| z7 | 26 | 27 | 1.040 | 0.6131 | 99.79% | 164 | 0.11 | 8601 | 0.328 | 0.05365 | 0.419131 | 0.104 | 0.056663 | 0.042 | 0.553 | 356.26 | 2.4 | 355.43 | 0.36 | 355.30 | 0.15 |
| 8) P99-WV-4K* – footwall crystal tuff (Wolverine/Lynx deposit; 439442 E, 6811694 N) | | | | | | | | | | | | | | | | | | | | | |
| z1 | 13 | 13 | 1.028 | 0.3036 | 99.64% | 95 | 0.09 | 4997 | 0.324 | 0.05367 | 0.419118 | 0.122 | 0.056640 | 0.049 | 0.559 | 357.11 | 2.8 | 355.42 | 0.43 | 355.16 | 0.17 |
| z2 | 30 | 31 | 1.012 | 0.7176 | 99.83% | 206 | 0.10 | 10912 | 0.319 | 0.05367 | 0.419219 | 0.058 | 0.056648 | 0.037 | 0.688 | 357.35 | 1.3 | 355.49 | 0.23 | 355.21 | 0.13 |
| z3 | 8 | 8 | 0.993 | 0.1955 | 99.45% | 62 | 0.09 | 3289 | 0.313 | 0.05365 | 0.419068 | 0.265 | 0.056651 | 0.053 | 0.477 | 356.41 | 6.0 | 355.38 | 0.86 | 355.23 | 0.18 |
| z4 | 14 | 13 | 0.933 | 0.3230 | 99.56% | 75 | 0.12 | 4073 | 0.294 | 0.05368 | 0.419464 | 0.111 | 0.056676 | 0.042 | 0.581 | 357.56 | 2.5 | 355.67 | 0.39 | 355.38 | 0.14 |
| z5 | 14 | 15 | 1.035 | 0.3394 | 99.72% | 123 | 0.08 | 6478 | 0.326 | 0.05380 | 0.430226 | 0.098 | 0.057996 | 0.042 | 0.619 | 362.77 | 2.2 | 363.34 | 0.36 | 363.43 | 0.15 |
| z6 | 11 | 10 | 0.923 | 0.2576 | 99.39% | 54 | 0.13 | 2941 | 0.291 | 0.05367 | 0.419219 | 0.162 | 0.056650 | 0.046 | 0.605 | 357.28 | 3.7 | 355.49 | 0.56 | 355.22 | 0.16 |
| z7 | 14 | 14 | 1.027 | 0.3292 | 99.63% | 91 | 0.10 | 4822 | 0.324 | 0.05365 | 0.419067 | 0.136 | 0.056650 | 0.045 | 0.534 | 356.44 | 3.1 | 355.38 | 0.46 | 355.22 | 0.16 |
| z8 | 16 | 16 | 0.984 | 0.3855 | 99.59% | 83 | 0.13 | 4425 | 0.310 | 0.05363 | 0.418876 | 0.124 | 0.056649 | 0.044 | 0.539 | 355.47 | 2.8 | 355.25 | 0.42 | 355.21 | 0.15 |
| 9) 18MM-102* – feldspar porphyritic rhyolite (Fisher zone; 433804 E, 6817011 N) | | | | | | | | | | | | | | | | | | | | | |
| z1 | 11 | 13 | 1.258 | 0.2493 | 99.03% | 37 | 0.20 | 1858 | 0.397 | 0.05369 | 0.418991 | 0.411 | 0.056601 | 0.056 | 0.612 | 357.98 | 9.3 | 355.33 | 1.33 | 354.92 | 0.19 |
| z3 | 7 | 8 | 1.164 | 0.1594 | 98.57% | 24 | 0.19 | 1264 | 0.367 | 0.05366 | 0.418982 | 0.378 | 0.056624 | 0.055 | 0.575 | 357.02 | 8.5 | 355.32 | 1.22 | 355.06 | 0.19 |
| z4 | 6 | 8 | 1.324 | 0.1394 | 98.13% | 19 | 0.22 | 963 | 0.417 | 0.05369 | 0.418983 | 0.493 | 0.056601 | 0.059 | 0.661 | 357.94 | 11.1 | 355.32 | 1.59 | 354.92 | 0.20 |
| z5 | 16 | 17 | 1.028 | 0.3862 | 99.38% | 55 | 0.20 | 2917 | 0.324 | 0.05364 | 0.418564 | 0.187 | 0.056595 | 0.046 | 0.515 | 355.93 | 4.2 | 355.02 | 0.62 | 354.89 | 0.16 |
| z6 | 59 | 71 | 1.217 | 1.3815 | 99.77% | 158 | 0.26 | 7982 | 0.384 | 0.05364 | 0.418831 | 0.094 | 0.056625 | 0.038 | 0.523 | 356.17 | 2.1 | 355.21 | 0.33 | 355.07 | 0.13 |
| z7 | 17 | 23 | 1.393 | 0.3940 | 99.41% | 62 | 0.20 | 3033 | 0.439 | 0.05374 | 0.419496 | 0.180 | 0.056610 | 0.045 | 0.537 | 360.38 | 4.1 | 355.69 | 0.60 | 354.97 | 0.15 |

[1] Sample numbers denoted with a * indicate the use of the ET2535 tracer solution, whereas the ET535 tracer was used for all other samples; UTM coordinates in NAD83 Zone 9U; z1, z2 etc. are labels for single zircon grains or fragments annealed and chemically abraded after Mattinson (2005); bold text indicates results used in weighted mean calculations

[2] Model Th/U ratio iteratively calculated from the radiogenic 208Pb/206Pb ratio and 206Pb/238U age

[3] Pb* and Pbc represent radiogenic and common Pb, respectively; mol % 206Pb* with respect to radiogenic, blank and initial common Pb

[4] Measured ratio corrected for spike and fractionation only; fractionation estimated at 0.17 ± 0.03%/a.m.u (ET535), for Daly analyses, based on analysis of NBS-981 and NBS-982 or internally corrected with ET2535

[5] Corrected for fractionation, spike, and common Pb; all common Pb was assumed to be procedural blank: 206Pb/204Pb = 18.042 ± 0.61%; 207Pb/204Pb = 15.537 ± 0.52%; 208Pb/204Pb = 37.686 ± 0.63% (all uncertainties 1σ)

[6] Errors are 2σ, propagated using the algorithms of Schmitz and Schoene (2007)

[7] Calculations are based on the decay constants of Jaffey et al. (1971); 206Pb/238U and 207Pb/206Pb ages corrected for initial disequilibrium in 230Th/238U using Th/U [magma] = 3
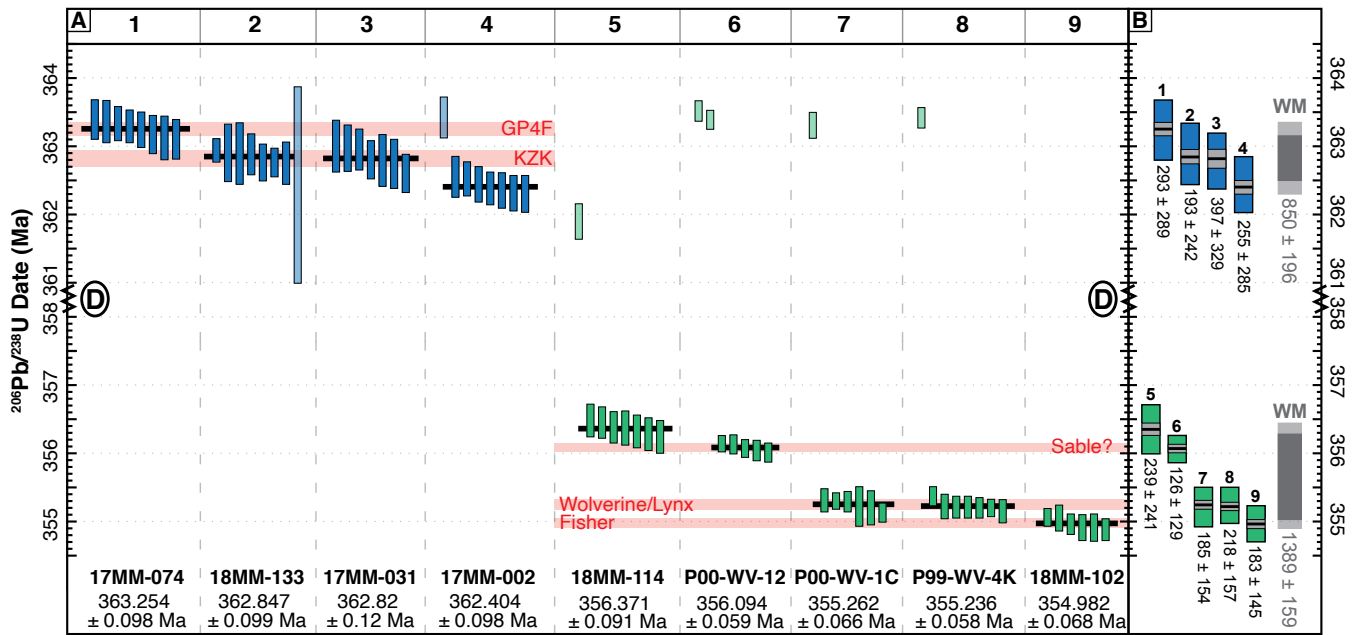
Fig. 14. Summary of chemical abrasion-thermal ionization mass spectrometer (CA-TIMS) U-Pb geochronological results in ranked order. A) Ranked U-Pb zircon CA-isotope dilution (ID)-TIMS geochronology results for the Kudz Ze Kayah formation (blue) and the Wolverine Lake group (green). Each vertical bar represents a single $^{206}$Pb/$^{238}$U date with maximum $2\sigma$ extents (Table 1). Horizontal black bars indicate the weighted mean $^{206}$Pb/$^{238}$U date. Lighter vertical bars are not included in the weighted mean calculation for each sample and, except for z1 in 18MM-133, are interpreted as xenocrysts. Horizontal pink lines indicate distinct time intervals of VMS mineralization based on $2\sigma$ uncertainties on the weighted mean date, indicated by the names of deposits from which rocks were sampled (red text). Broken Y-axis scale from 361 to 358 Ma indicates a period of deformation (D), represented by an angular unconformity between the two stratigraphic successions. Bold numbers correspond to sample numbers in Figures 4 through 8 and Table 1. B) Summary of age distributions ($\Delta t$) for each sample (blue = Kudz Ze Kayah formation; green = Wolverine Lake group) and the total minimum and maximum durations based on weighted mean $^{206}$Pb/$^{238}$U dates (WM), $^{206}$Pb/$^{238}$U dates, and their associated $2\sigma$ uncertainties. Vertical boxes represent the $\Delta t$ for each category. Durations given in k.y.

## Wolverine Lake group

*Fisher feldspar porphyry (18MM-102):* Zircon from feldspar porphyritic rocks (18MM-102) in the Fisher zone are typically euhedral, prismatic grains between 80 and 140 $\mu$m in length with high aspect ratios (2:1 to 3:1; Fig. 12B, App. Fig. A4). The zircon grains are generally CL-bright and display oscillatory and patchy sector zoning that is both CL-bright and CL-dark. The The CA-ID-TIMS analytical results are concordant with high Th/U (1.02–1.39, n = 6) and a weighted mean $^{206}$Pb/$^{238}$U date of 354.982 ± 0.068 Ma ($2\sigma$; MSWD = 0.93; n = 6; Table 1; Fig. 13E). This U-Pb date is inferred to be the crystallization age of this rock and the age mineralization in the Fisher zone. The LA-ICP-MS data yield concordant results with variable Th/U (0.24–3.2) and a weighted mean $^{206}$Pb/$^{238}$U date of 355.5 ± 1.8 Ma ($2\sigma$; MSWD = 1.19; n = 29), which overlaps the CA-ID-TIMS date within uncertainty. Ten zircon grains have older U-Pb dates between ca. 367 to 379 Ma (n = 9) and 1811 Ma (n = 1), where all are interpreted as xenocrysts.

*Wolverine/Lynx footwall (P99-WV-4K):* Zircon grains from a feldspar ± quartz crystal tuff in the footwall of the Wolverine/Lynx deposit are euhedral and ~80 to 150 $\mu$m in length with aspect ratios ~2:1 (Fig. 12B, App. Fig. A4). The zircon crystals typically have oscillatory zoning with minor sector zoning (e.g., z3). The CA-ID-TIMS data shows seven concordant zircon fractions with high Th/U (0.92–1.03) and a weighted

mean $^{206}$Pb/$^{238}$U date of 355.236 ± 0.058 Ma ($2\sigma$; MSWD = 0.85; Table 1; Fig. 13F), interpreted to be the eruption age of the rock and the approximate age of the Wolverine/Lynx VMS deposit. Zircon fraction z5 is interpreted as a xenocryst due to its concordant U-Pb date of ~363.4 Ma. The LA-ICP-MS results are concordant and yield highly variable Th/U (0.23–5.4) and correspond to a weighted mean $^{206}$Pb/$^{238}$U date of 353.3 ± 1.7 Ma ($2\sigma$; MSWD = 0.97; n = 37), which is slightly younger outside of uncertainty than the CA-ID-TIMS date. Four grains have older $^{206}$Pb/$^{238}$U dates between ca. 366 and 373 Ma and are interpreted as xenocrysts.

*Wolverine/Lynx feldspar porphyry (P00-WV-1C):* A feldspar porphyritic rock (P00-WV-1C) in the Wolverine/Lynx deposit footwall yielded zircon that is euhedral and relatively small (~60–90 $\mu$m in length) with low aspect ratios (1:1 to 2:1). The zircon grains display oscillatory zoning and sector zoning shown by CL-bright zones (e.g., z2 and z3; Fig. 12B, App. Fig. A4). Results from CA-ID-TIMS analyses reveal zircon grains that are concordant with high Th/U (0.90–1.1) and a weighted mean $^{206}$Pb/$^{238}$U date of 355.262 ± 0.066 Ma ($2\sigma$; MSWD = 0.99; Table 1; Fig. 13G); this date is inferred as the crystallization age of the rock and the age of mineralization in the Wolverine/Lynx deposit. One zircon fraction (z6) is inferred to be a xenocryst with a concordant U-Pb date of ~363.3 Ma. The LA-ICP-MS analytical results are concordant and yield variable Th/U (0.14–3.7) with a weighted mean $^{206}$Pb/$^{238}$U date

of 352.8 ± 2.2 Ma ($2\sigma$; MSWD = 1.07; $n$ = 25); this date is slightly younger outside of uncertainty than the CA-ID-TIMS date. Three older grains gave dates of ca. 370 to 371 Ma ($n$ = 2) and a $^{207}$Pb/$^{206}$Pb date of 1105 Ma ($n$ = 1), which are all interpreted to be xenocrystic zircon.

*Sable quartz-feldspar porphyry (P00-WV-12):* Zircon grains in a quartz-feldspar porphyritic rock (P00-WV-12) in the Sable zone are euhedral and prismatic with grain sizes between 100 and 250 $\mu$m in length. The grains have the highest aspect ratios of samples in the Wolverine Lake group, ranging between ~2:1 and 4:1, and show oscillatory zoning with CL-bright cores and CL-dark rims (Fig. 12B, App. Fig. A4). The CA-ID-TIMS data show five concordant zircon fractions with relatively low Th/U (0.45–0.70) and a weighted mean $^{206}$Pb/$^{238}$U date of 356.094 ± 0.059 Ma ($2\sigma$; MSWD = 0.67; Table 1; Fig. 13H), interpreted as the crystallization age of the rock. Two zircon fractions (z5 and z7) have high Th/U (1.15–1.25) and concordant U-Pb dates of ~363.4 and ~363.5 Ma, which are interpreted as xenocrysts. The LA-ICP-MS data give concordant results with variable Th/U (0.15–2.2) and a weighted mean $^{206}$Pb/$^{238}$U date of 354.6 ± 2.1 Ma ($2\sigma$; MSWD = 1.05; $n$ = 22), which overlaps within error of the CA-ID-TIMS date. Five zircon grains have older dates between ca. 366 and 369 Ma and are interpreted as xenocrysts.

*Lower Wolverine Lake group (18MM-114):* Zircon grains from this sample (18MM-114) are euhedral and range from near-equant (aspect ratio = ~1:1) to prismatic (~2:1 to 4:1) morphologies that are 60 to 80 and 80 to 200 $\mu$m in length, respectively (Fig. 12B, App. Fig. A4). The zircon grains typically display oscillatory zoning with CL-bright core zones. The CA-ID-TIMS analytical results are concordant with relatively low Th/U (0.25–0.35, 0.80) and a weighted mean $^{206}$Pb/$^{238}$U date of 356.371 ± 0.091 Ma ($2\sigma$; MSWD = 0.53; $n$ = 7; Table 1; Fig. 13I), interpreted as the eruption age of this rock and the onset of volcanism in the Wolverine Lake group. The LA-ICP-MS analytical results are concordant with variable Th/U (0.16–2.2) and a weighted mean $^{206}$Pb/$^{238}$U date of 359.5 ± 2.0 Ma ($2\sigma$; MSWD = 1.5; $n$ = 31), which is distinctly older outside of uncertainty to the CA-ID-TIMS date. This sample contains seven zircon grains that are significantly older than the weighted mean date, including ca. 372 Ma ($n$ = 1) and $^{207}$Pb/$^{206}$Pb dates of 1062 Ma ($n$ = 1), 1192 Ma ($n$ = 1), 1721 to 1766 Ma ($n$ = 3), and 1886 Ma ($n$ = 1); all of these grains are interpreted to be xenocrysts.

## Volcano-Sedimentary Accumulation Rates and Volume Estimates

Rates of volcano-sedimentary accumulation in submarine settings are dependent on the character of volcanism, tectonic and depositional setting, and proximity to the continental slope and/or arc edifice (e.g., Karig and Moore, 1975; Carey and Sigurdsson, 1984; Díaz-Asencio et al., 2019). Quantitative estimates of volcaniclastic sedimentation rates on the modern seafloor are typically between 300 and 1000 m/m.y. for Eocene continental margin basins and younger early intra-arc rift settings (Karig and Moore, 1975; Clift, 1995; Marsaglia et al., 1995; Carey, 1999). Rates for background sedimentation devoid of volcanism are typically lower and in continental shelf environments, such as in the Gulf of Mexico, where rates decrease from the slope to the deeper abyssal plain areas (~130–

180 m/m.y. to ~30–50 m/m.y.; Santschi and Rowe, 2008; Díaz-Asencio et al., 2019). The Middle Valley sedimented rift in the Juan de Fuca Ridge contains background Holocene sedimentation rates of 55 to 65 m/m.y., but much higher rates related to Pleistocene turbidite influx have been also recorded at this site (400 m/m.y.; Goodfellow and Franklin, 1993). Volumetric rates for subaerial, silicic volcanic eruptions in continental and oceanic tectonic settings range from 2 to 11,550 km$^3$/m.y. (median = 921 km$^3$/m.y.; $n$ = 79; White et al., 2006, and references therein). Moreover, the volcano-sedimentary accumulation rates in the literature vary significantly between 30 and 1,000 m/m.y. and are dependent on the sediment source and the association with active submarine volcanism (e.g., Karig and Moore, 1975; Díaz-Asencio et al., 2019).

Stratigraphic reconstructions and new CA-ID-TIMS U-Pb results provide constraints for estimations of volcano-sedimentary accumulation rates and volume estimates for intra-basinal facies in the Kudz Ze Kayah formation and Wolverine Lake group. Due to the lack of drilling constraints and minimal outcrop exposure in low-lying areas, we have simplified the volcanic facies in the entire Kudz Ze Kayah formation and Wolverine Lake group footwall into discrete units, although both are composed of numerous individual eruptions that were likely deposited at much faster rates. In the case of the Kudz Ze Kayah formation and Wolverine Lake group, the major map units are relatively continuous along strike, and are estimated to have strike lengths of at least 15 and 23 km, respectively (Figs. 4, 5). The lateral continuity of these basins is similar in basin structure to various parts of the Okinawa Trough (e.g., Arai et al., 2017; Minami et al., 2020), which has been interpreted as the closest modern analogue to the Finlayson Lake district (Piercey et al., 2001). The stratigraphic locations of U-Pb samples are thus extrapolated to similar locations in all cross sections and rates are calculated based on the thickness of the column divided by the total $\Delta$t for the entire unit, unless otherwise noted. For each case, the minimum $\Delta$t is the smallest difference between the weighted mean $2\sigma$ envelopes and the maximum $\Delta$t is the total range of single crystal dates, including the $2\sigma$ error. The Wolverine Lake group has been attributed to forming in a basin of at least ~14 by 10 km (Bradshaw et al., 2008); however, we recognize a much greater strike length of ~23 km (Fig. 3). Volumetric estimates for the regional units are calculated using a modified method of Kokelaar and Busby (1992) and Hudak et al. (2003) to account for a basin shape that is assumed to have a length greater than its width. Thus, we use the formula for an elliptical cylinder ($V = \pi abh$), where $a$ is half the strike length, $b$ is 70% of $a$, and $h$ is the dip-corrected unit thickness (Fig. 8). Moreover, these calculations represent minimum estimates for both rates and volumes due to post-depositional lithification, deformational compression, and erosion (e.g., Kokelaar and Busby, 1992; Hudak et al., 2003).

The U-Pb dates for the Kudz Ze Kayah formation indicate that volcanism lasted <1 m.y. and accumulated with rates between 350 and 1,900 m/m.y. (Table 2). Taking only the facies thickness of ~600 m and $\Delta$t ~400 k.y. between the GP4F and Kudz Ze Kayah deposits, higher calculated rates between 1,000 and 2,900 m/m.y. are observed. Repeated occurrences of thick (>10- to 50-m), unsorted to poorly sorted crystal and lapilli-rich tuffs at and in between the two VMS deposits

may indicate that these units were deposited as volcaniclastic mass-flows, which have been interpreted to represent rapid emplacement and burial rates during subaqueous volcanic eruptions (e.g., App. Fig. A1; McPhie et al., 1993; White, 2000). Estimated volumes of facies along the ~15-km strike length yield an average of ~150 km³ of basin fill, which correspond to time-resolved rates between 110 and 180 km³/m.y. In the Wolverine Lake group, the footwall volcano-sedimentary facies reflect up to 1.5 m.y. of deposition that accounts for average accumulation rates of ~800 to 1,400 m/m.y., similar to those in the Kudz Ze Kayah formation (Table 2). Facies below the stratigraphic level of the Sable zone (i.e., sample P00-WV-12), not including the lowermost quartzofeldspathic meta-sandstone, were deposited at a rapid rate of between 2,300 and 7,800 m/m.y. ($\Delta t$ = ~150–400 k.y.) and are interpreted to be a result of volcanic and sediment influx by mass transport complexes or turbidity currents similar to those observed in the hanging wall of the Wolverine deposit (Piercey et al., 2016). The longer strike length (~23 km) of the Wolverine Lake group strata alone indicates larger volumes of basin fill than in the Kudz Ze Kayah formation, yielding a minimum volume of ~440 km³ with rates between 280 and 360 km³/m.y. (Table 2). The total volcanic contributions in the Wolverine Lake group are approximately 1.8 times greater than argillite, whereas in the Kudz Ze Kayah formation, volcanic facies are much more abundant (~3.8 times) than siltstones and argillites.

## Discussion

The new lithostratigraphic and U-Pb geochronological constraints for the Finlayson Lake VMS district provide insights into the timing and duration of VMS mineralization and rates of basin-scale volcano-sedimentary depositional processes in an ancient continental margin setting. Our results provide the first robust dates, absent of Pb loss effects and inheritance, for all known felsic-hosted, Zn-enriched VMS deposits in the Finlayson Lake district and provide insight into depositional rates

at a resolution that has not been previously documented in the ancient geologic record. These results provide improved stratigraphic constraints for the Kudz Ze Kayah formation and Wolverine Lake group and directly impact regional correlations throughout the Yukon-Tanana terrane. The discussion below highlights the importance of integrating detailed stratigraphic and high-precision CA-ID-TIMS geochronological results to establish links between depositional rates and replacement-style mineralization in seafloor and subseafloor environments.

### Timing and duration of felsic-hosted VMS mineralization

The age and duration of mineralizing processes in VMS districts is critical to understanding the development of hydrothermal systems in the upper crust and identifying prospective areas for future exploration; however, depositional rates are challenging to determine in the ancient record, and this limits our ability to compare rates of deposit formation between modern seafloor massive sulfide (SMS) and ancient VMS systems. Current U-Pb zircon geochronology methods, coupled with precise stratigraphic controls, can constrain the lower and upper age extents of VMS mineralization within a district (e.g., Bleeker and Parrish, 1996; Bleeker et al., 1999; Ross et al., 2014; Mortensen et al., 2015; Oliver et al., 2021), but do not allow for direct dating of hydrothermal mineralization except in the exceptionally rare cases where hydrothermal zircon is observed (e.g., Iberian Pyrite Belt; Nesbitt et al., 1999). Therefore, quantifying the age and duration of mineralization has historically been challenging due to the uncertainties on U-Pb dates (>0.2% at best on individual zircon crystals before 2010; Schoene, 2014) that often are much greater than the lifespan of hydrothermal systems (~10 k.y. to 1 m.y.; e.g., Cathles et al., 1997; Barrie et al., 1999; Hannington et al., 2005). With modern CA-ID-TIMS U-Pb zircon geochronology, however, the uncertainties are now typically <0.1% (Schoene and Baxter, 2017) and stratigraphically bracketed U-Pb dates in a VMS deposit (i.e., stratigraphically above and

Table 2. Summary of Calculated Volcano-Sedimentary Accumulation Rates

| Location[1] | Thickness of section (m)[2] | Corrected thickness (m)[3] | Average linear rate (m/m.y.)[4] | Peak linear rate (m/m.y.)[5] | Average volume of unit (km³)[6] | Volcanic/argillite volumes (km³) | Average volumetric rate (km³/m.y.)[6] |
|---|---|---|---|---|---|---|---|
| *Kudz Ze Kayah formation* | | | | | | | |
| A-A' | 560 | 380 | 360–580 | 1,000–2,900 | 148 | 117 / 31 | 112–179 |
| B-B' | 1,380 | 870 | 830–1,330 | | | | |
| C-C' | 1,370 | 1,240 | 1,190–1,900 | | | | |
| D-D' | 950 | 950 | 910–1,460 | | | | |
| E-E' | 1,730 | 1,290 | 1,240–1,980 | | | | |
| | | | | | | | |
| *Wolverine Lake group* | | | | | | | |
| F-F' | 1,710 | 1,240 | 800–1,010 | 2,300–7,800 | 438 | 280 / 156 | 283–356 |
| G-G' | 1,680 | 1,500 | 970–1,220 | | | | |
| H-H' | 2,120 | 1,770 | 1,150–1,440 | | | | |

[1]Location of sections correspond to lines in Figs. 4-7, and columns in Fig. 8
[2]Thicknesses measured from cross sections in Figs. 6 and 7; Grass Lakes plutonic suite is omitted; Wolverine Lake group footwall only
[3]Corrected thicknesses do not include basal sedimentary units SLT and MDS (Kudz Ze Kayah formation), footwall unit Wcl and hanging wall units RCF, FRB, and MFV (Wolverine Lake group)
[4]Calculated using total $\Delta t$ ($\pm 2\sigma$) for the corrected thickness of each section
[5]Peak rates for Kudz Ze Kayah formation between GP4F and Kudz Ze Kayah deposits (~600 m), and Wolverine Lake group between lower footwall and Sable zone (~1,000 m)
[6]Volumes for Kudz Ze Kayah formation use the total thickness of the section, whereas Wolverine Lake group calculations use the corrected thickness; see text for discussion of volume parameters; average volumetric rate = average volume*$\Delta t$ ($\pm 2\sigma$)

below, or below and cross cutting the VMS deposit) are at much higher resolution than dates that have been obtained from direct dating of the mineralization event using U-Pb or other isotopic methods (e.g., Mathur et al., 1999; Nesbitt et al., 1999; Nozaki et al., 2014).

Zircon from nine U-Pb samples from the Kudz Ze Kayah formation and Wolverine Lake group were used to define the lower and upper temporal bounds of each rock succession and precise ages of VMS deposits in each unit (Figs. 13–15). Zircon grains dated from four samples of volcaniclastic rocks from the Kudz Ze Kayah formation yield tightly constrained weighted mean $^{206}Pb/^{238}U$ dates (ca. 363.3–362.4 Ma) that distinguish the ages of VMS mineralization in the GP4F, ABM, and Krakatoa zones, and the absolute duration of volcanic activity ($\Delta t$ = 0.65–1.0 m.y.; Fig. 14). At lower stratigraphic levels, the earliest-known volcanic phase in the Kudz Ze Kayah formation is 363.254 ± 0.098 Ma (17MM-074), interpreted to be the age of the GP4F deposit. Approximately 600 m stratigraphically above GP4F, both the Krakatoa and ABM zones of the Kudz Ze Kayah deposit yield nearly identical dates of 362.847 ± 0.099 Ma (18MM-133) and 362.82 ± 0.12 Ma (17MM-031), respectively. The last phase of felsic volcanism in the Kudz Ze Kayah formation occurred at 362.404 ± 0.098 Ma (17MM-002), which was determined from zircon in a felsic crystal tuff that is ~250 m stratigraphically above the Kudz Ze Kayah deposit. Similarly, the new U-Pb zircon results for five rocks in the Wolverine Lake group (ca. 357.5–354.9 Ma) constrain the timing of mineralization for the Wolverine/Lynx, Sable, and Fisher zones, and define the duration of volcano-sedimentary activity for the footwall facies ($\Delta t$ = 1.2 to 1.5 m.y.; Fig. 13). Following a period of sedimentation at ca. 357.5 Ma (Fig. 15; Murphy et al., 2006), felsic volcanism in the lower footwall unit began at 356.371 ± 0.091 Ma (18MM-114). Approximately 1,000 m of crystal tuffs and argillites separate the lower footwall from the Sable zone, which was cut by a quartz-feldspar porphyritic intrusion at 356.094 ± 0.059 Ma (P00-WV-12). The Wolverine/Lynx zone is ~2 km northwest along strike from the Sable zone, where overlapping dates for a crystal tuff (355.236 ± 0.058 Ma; P99-WV-4K) and a feldspar-porphyritic rhyolite (355.262 ± 0.066 Ma; P00-WV-1C) define the age of the Wolverine deposit footwall and the maximum age of the VMS mineralization (Piercey et al., 2008). Stratigraphy in the Fisher zone, approximately 9 km along strike to the northwest of the Wolverine/Lynx zone, was intruded by a large feldspar-porphyritic stock at 354.982 ± 0.068 Ma and defines the latest phase of volcanism in the Wolverine Lake group footwall unit, interpreted to be the minimum estimate for VMS mineralization.

The strong lateral continuity of lithofacies in the Kudz Ze Kayah formation and Wolverine Lake group, combined with new high-precision U-Pb dates for VMS-bearing stratigraphy, is interpreted to suggest that volcanism and associated VMS mineralization occurred at distinct periods during the life of the back-arc basin (Table 1; Fig. 14). For example, CA-ID-TIMS dates for the GP4F (sample 17MM-074) and Kudz Ze Kayah deposits (17MM-031 and 18MM-133) show that the maximum extent of $2\sigma$ errors for weighted mean $^{206}Pb/^{238}U$ dates are ~200 and ~250 k.y., respectively, indicating that deposition of mineralization occurred over 200 to 250 k.y. (Fig. 14). In the Wolverine Lake group, porphyritic rocks have

been shown to be either pre-mineralization (quartz-feldspar porphyritic rocks) or syn- to post-mineralization (feldspar porphyritic rocks; Piercey et al., 2008), thus providing maximum and minimum ages for mineralization. The quartz-feldspar porphyritic rocks intruded at ca. 356.1 Ma, whereas the feldspar-porphyritic rocks intruded between ca. 355.2 and 355.0 Ma; each sample accounts for a maximum of ~120 to 140 k.y. of $2\sigma$ uncertainty on the weighted mean date. These results further indicate that deposition of VMS mineralization for the Wolverine/Lynx (P00-WV-1C and P99-WV-4K) and Fisher zones (18MM-102) occurred over ~150 and 140 k.y., respectively (Fig. 14).

Accumulation rates for massive sulfide horizons in ancient VMS deposits in the literature are exceptionally rare (e.g., Bleeker and Parrish, 1996) but critical to facilitate comparisons to modern SMS deposits (e.g., Jamieson et al., 2014) and to provide a broader understanding of the rates of SMS/VMS formation in modern and ancient settings. The calculated rates were determined as follows: 1) the maximum and minimum age ranges for a given deposit based on stratigraphic and cross cutting relationships were determined; and 2) the massive sulfide tonnage was then divided by these age ranges to determine the minimum and maximum accumulation rates. Estimates for the Kudz Ze Kayah deposit (~19 Mt; van Olden et al., 2019) suggest mass accumulation rates of ~75 to 800 t/yr, and much lower rates of ~8 t/yr for GP4F (~1.5 Mt; Peter et al., 2007). Estimated depositional rates for the Wolverine deposit (~5.2 Mt; Regan, 2007) are between ~40 and 200 t/yr. These rates are comparable to estimates for the Kidd Creek deposit, where average rates were suggested to be between 10 and 100 t/yr and peak rates reached as high as 1,000 t/yr (Bleeker and Parrish, 1996), and for modern hydrothermal deposits where mass accumulation rates lie between 1 and 794 t/yr (e.g., Jamieson et al., 2014). Our data further indicate the following: 1) it is possible to compare ancient VMS accumulation rates with modern SMS accumulation rates using high-resolution U-Pb geochronology; 2) rates are similar in ancient deposits when compared to modern deposits; however, the ancient deposits are limited to the Finlayson Lake district (this study) and Kidd Creek (Bleeker and Parrish, 1996); and 3) rate resolution between modern SMS and ancient VMS can only be determined using high-precision geochronology methods, like the CA-ID-TIMS data presented herein.

### Relationship between Kudz Ze Kayah and Wolverine Lake basins

The Kudz Ze Kayah formation and Wolverine Lake group contain volcano-sedimentary facies that are similar in texture and geochemical affinity; however, the units represent two distinct periods of magmatism and deposition along the western Laurentian continental margin (Piercey et al., 2001; Murphy et al., 2006). Our U-Pb results show that the Kudz Ze Kayah formation and Wolverine Lake group formed between ca. 363.3 and 362.4 and ca. 357.5 and 354.9 Ma, respectively (Figs. 13, 14). Further, Proterozoic zircon xenocrysts, as shown by LA-ICP-MS results, are present in both Kudz Ze Kayah formation and Wolverine Lake group footwall samples and are interpreted to reflect melting of a crustal substrate with Laurentian affinity (e.g., Snowcap assemblage; Piercey and Colpron, 2009; Fig. 15; App. Fig. A6, Table A2); these

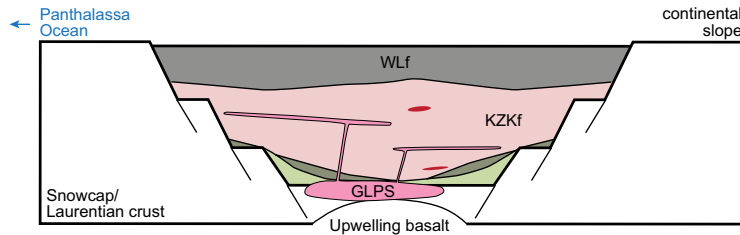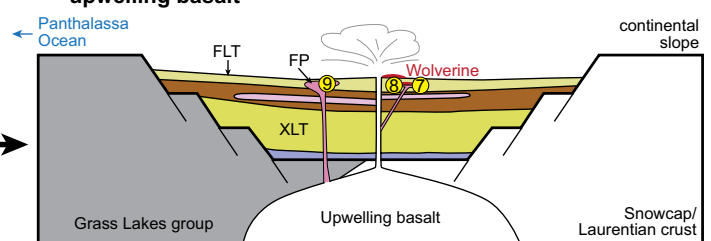## Deposition of the Kudz Ze Kayah formation (ca. 363.3 to 362.4 Ma)
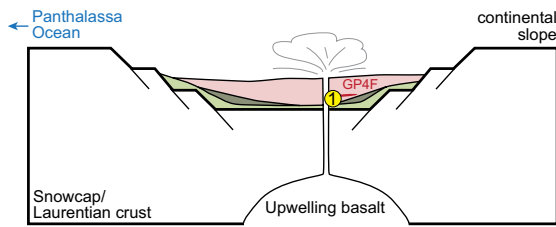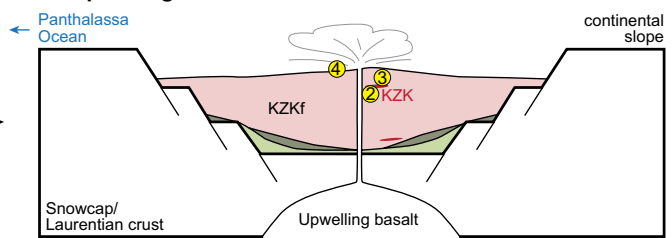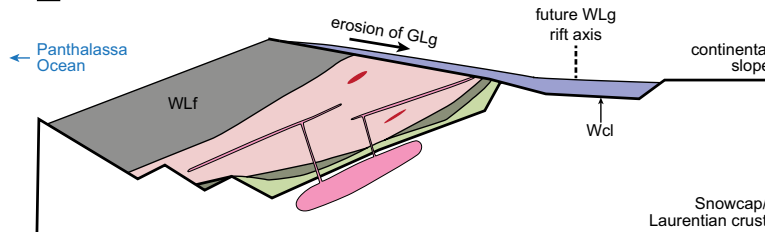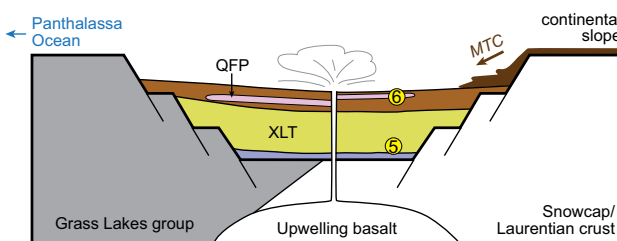


Fig. 15. Schematic diagrams illustrating the evolution of Upper Devonian and Early Mississippian submarine back-arc basins in the Finlayson Lake volcanogenic massive sulfide (VMS) district, Yukon-Tanana terrane. A) Early-stage rifting resulting in the deposition of the Kudz Ze Kayah formation (KZKf), where felsic volcaniclastic rocks were deposited in association with hydrothermal upwelling to form the GP4F deposit. B) Upwelling basalt and accelerated extension resulting in tectonic subsidence provide favorable conditions for rapid volcaniclastic accumulation, hydrothermal activity, and subseafloor replacement-style mineralization in the Kudz Ze Kayah deposit (ABM and KKT zones) at ca. 362.8 Ma. C) Waning of the rifting leads to eruption and deposition of alkalic basalts and mudstones in the Wind Lake formation (WLf) above the Kudz Ze Kayah formation, which are then cut by plutons and dikes of the Grass Lakes plutonic suite (GLPS). D) A period of $D_1$ deformation causes penetrative $S_{1-GLg}$ fabrics in the Grass Lakes group (GLg). The rocks are uplifted, tilted, and eroded into a new, incipient back-arc basin (Wolverine Lake group; WLg), transporting zircon with ages ca. 363.5 to 358 Ma into the new basin contained in unit Wcl (Murphy and Piercey, 1999; Murphy et al., 2006). E) Rifting resumes and volcaniclastic rocks (unit XLT) are deposited in thick accumulations, partly on top of the older rift stratigraphy. Thick argillite packages are deposited from mass transport complexes and/or turbidity currents from the continental slope as a result of rapid extension and steep basin topography. These strata are intruded by quartz-feldspar porphyritic sills and dikes at ca. 356.1 Ma. F) Felsic volcaniclastic rocks (unit FLT) are deposited and intercalated with argillite. Rapid deposition of footwall tuffs and feldspar porphyritic intrusive rocks between ca. 355.2 and 355.0 Ma, coupled with hydrothermal upwelling, facilitated subseafloor and intermittent seafloor mineralization in the Wolverine deposit and Fisher zone. Yellow symbols and numbers correspond to U-Pb samples and stratigraphic locations as in Figures 4 through 8 and 14. For simplicity in panels (E) and (F), units in the Grass Lakes group are shaded to a single gray color.

results also concur with previous geochronology work in the Finlayson Lake district (Grant, 1997; Murphy et al., 2006; Piercey et al., 2008). From CA-ID-TIMS results, xenocrystic zircon in three of five rocks from the Wolverine Lake group indicate that Early Mississippian magmatic rocks in the group record assimilation or mixing with sources that contain zircon with dates coeval with the stratigraphically lowest parts of the Kudz Ze Kayah formation (ca. 363.5–363.3 Ma; $n$ = 3; Table 1; Figs. 13, 14). Similarly, one xenocrystic zircon (ca. 361.9 Ma) was dated in sample 18MM-114 from the lower Wolverine Lake group footwall (unit XLT; Fig. 5) and has an age similar to those for the Grass Lakes plutonic suite that intrudes the Grass Lakes group (Murphy et al., 2006).

These observations are important for three reasons. First, the stratigraphic position of the crystal tuff unit (XLT) in the lower Wolverine Lake group, which contains the ca. 361.9 Ma xenocryst, suggests that erosion or mixing of the underlying Grass Lakes group units was more widespread and was not just recorded in the basal sedimentary rocks (i.e., Wcl unit) of the group (e.g., Murphy and Piercey, 1999); however, it is also possible that this grain was inherited by the magmas that were responsible for generating the crystal tuffs (Fig. 3). Second, older ca. 363.5–363.3 Ma xenocrysts in feldspar porphyritic, quartz-feldspar porphyritic, and tuffaceous units at the highest levels of Wolverine Lake group stratigraphy indicate that zircon was either entrained by magmas through crustal assimilation or, in the case of the felsic crystal tuff (P99-WV-4K), mixed by sedimentary processes either by passing through zones of the lower Kudz Ze Kayah formation or zones of the basal sedimentary rock unit (Wcl) that contained older zircon grains from the Kudz Ze Kayah formation (Fig. 15). Third, the oldest xenocrysts from CA-ID-TIMS results are among the oldest Late Devonian dates presented in this study and could indicate that there are older Late Devonian rocks (>363.5 Ma) beneath the GP4F deposit (ca. 363.3 Ma) that have yet to be recognized. These results illustrate that there may be more important basement connections and crustal inheritance between the two basins at depth that, until now, have not been recognized.

*Basin-scale accumulation rates and comparisons to modern environments*

Our U-Pb results are the first to constrain the rates of magmatism and volcano-sedimentary deposition in an ancient Paleozoic seafloor VMS environment, with accumulation rates of ~350 to >2,000 m/m.y. in the Finlayson Lake district. These estimates are greater than those observed on the modern seafloor, such as in continental margin basins and early intra-arc rift settings (300–1,000 m/m.y.; Karig and Moore, 1975; Clift, 1995; Marsaglia et al., 1995; Carey, 1999). Volcano-sedimentary accumulation rates in deep marine back-arc basins, the interpreted setting of the Finlayson Lake district, are dependent on the volcanic style (e.g., deep- vs. shallow-level eruptions, degree of explosivity; Gibson et al., 1999; Allen and Stewart, 2003; Cas and Simmons, 2018) and the stage of back-arc development (e.g., Carey and Sigurdsson, 1984). Furthermore, the source and eruptive style of volcanoes can greatly influence the quantity of particles available for deposition, especially in submarine environments where hydrostatic pressure and the presence of water affect the

separation and distribution of facies generated by pyroclastic eruptions (Cas and Simmons, 2018). Subaerial systems are known to facilitate large-volume silicic eruptions (>$10^3$ km³) that are observed to deliver volcanic ash to the water column by ash plumes (e.g., Mt. Pinatubo; Bryan et al., 2010, and references therein) or by pyroclastic eruptions that breach the seawater interface (e.g., Soufrière Hills volcano, Montserrat; le Friant et al., 2009). We do not envision subaerial arc eruptions to have had a significant impact on volcanic facies in the units studied here for three primary reasons. First, there is little evidence for shallow water textural features in the volcanic facies (e.g., tractional current-related bedforms, welding) as would be expected of ash columns entering a back-arc basin, suggesting that rocks herein were formed below the storm wave base (Gibson et al., 1999). Second, the rocks do not preserve features consistent with eruption in a subaerial environment, such as accretionary lapilli (Piercey et al., 2001; 2016). Lastly, the district contains local- to map-scale features in volcanic and sedimentary facies that indicate facies deposition from turbidity currents and/or debris flows. Examples include normal grading of sand- to mud-rich facies (i.e., Kudz Ze Kayah-Wind Lake formation; Fig. 4), tuff or mudstone bedforms in the Wolverine Lake group footwall (Fig. 5), and alternating tuff-argillite sequences attributed to turbidity currents in the Wolverine Lake group hanging wall (Piercey et al., 2016). These geologic features are much more consistent with having formed during the early-rift stages of back-arc development where steep topography was created on the seafloor, leading to the development of a basin architecture that facilitated abundant submarine eruptions and mass transport complexes or turbidity current-related deposits (Fig. 15; Carey and Sigurdsson, 1984; Clift, 1995). Our new U-Pb dates and associated accumulation rates, together with chemical and regional facies associations, also suggest that the Kudz Ze Kayah formation and Wolverine Lake group were formed in incipient back-arc basins with an early-rift architecture, which then facilitated rapid, submarine volcanism and debris flows and/or turbidity currents, likely coupled with rapid subsidence (Fig. 15). Together, these characteristics suggest that the facies that directly host abundant VMS mineralization were deposited rapidly in an evolving back-arc basin.

Rapid emplacement of volcanic facies on the seafloor facilitates the formation of a water-saturated interface where unconsolidated sediments and rock fragments dominate (Cas and Wright, 1987; Doyle and Allen, 2003). This water-saturated interface facilitates a chaotic volcanic environment if subsequent lavas and/or subvolcanic intrusions are emplaced, which would then be subjected to quench fragmentation and creation of autoclastic and fractured coherent facies (e.g., McPhie and Allen, 1992; Cas and Simmons, 2018). This layer of unconsolidated sediment should continue to be present with further rapid volcanic and volcano-sedimentary emplacement, especially if large volumes of sediment are supplied to the basin in rapid succession, which appears to have been the case in both the Kudz Ze Kayah and Wolverine basins based on our depositional rate calculations. Contemporaneous hydrothermal upwelling within a seafloor-subseafloor environment like the above leads to conditions that are optimal for deposition of sulfides in both the seafloor and subseafloor setting as the metal-rich hydrothermal fluids mix with seawa-

ter in the bottom waters of the ocean, as well as with fluids trapped in pore spaces and/or fractures in clastic and coherent facies, respectively (Doyle and Allen, 2003; Piercey, 2015). We have demonstrated that rapid volcanic emplacement processes have occurred in the Finlayson Lake district and are associated with VMS deposits; however, it is uncertain what their role is in creating replacement-style mineralization as predicted above. Below, we evaluate the role of emplacement rate and sulfide emplacement style using deposits in the Finlayson Lake district.

### Subseafloor replacement-style mineralization and potential relationships to accumulation rates

Subseafloor replacement is recognized as an important process in the formation of many VMS deposits globally (Doyle and Allen, 2003); however, in the ancient record, the geologic information required to document these processes can often be obscured due to post-depositional tectonic events, such as metamorphism and deformation (Allen et al., 2002; Piercey, 2015; Tornos et al., 2015). Replacement textures in VMS systems are typically observed as sulfide infiltration into either porous volcano-sedimentary facies or coherent and/or autoclastic lavas or subvolcanic intrusions (Doyle and Allen, 2003). The relatively intact stratigraphy in the Finlayson Lake district hosts at least three Zn-enriched VMS deposits that exhibit various primary textural and facies characteristics of subseafloor replacement-style mineralization processes (e.g., Fig. 16; Peter et al., 2007; Bradshaw et al., 2008). Previous workers have suggested subseafloor replacement was an important process in the genesis of some of the Finlayson Lake deposits (Peter et al., 2007; Bradshaw et al., 2008), and we provide additional evidence herein. For example, at Wolverine, the Zn-Pb-Fe–rich sulfides have textures that resemble partial or complete replacement of carbonaceous argillite and minor felsic tuff beds (Fig. 16A, B), filling fractures in coherent porphyritic intrusions (Fig. 16C), and microscale bud-by-bud replacement of framboidal sulfides with metal-rich sulfides (Peter et al., 2007; Bradshaw et al., 2008; Piercey, 2015). Replacement textures in the GP4F deposit include sulfide deposition subparallel to bedding in volcaniclastic rocks and relict lapilli and/or crystal fragments in the sulfide mineralization (Fig. 16D-F; Peter et al., 2007). The Kudz Ze Kayah deposit exhibits many of the same replacement characteristics, including relicts of rhyolite fragments or lapilli in sulfide interpreted to reflect partial to complete replacement of primary volcaniclastic facies by sulfide minerals (Fig. 16G, I-K), fracture infill of sphalerite in coherent rhyolite (Fig. 16H), and the presence of sulfides that have contacts discordant to bedding surfaces (Fig. 16L). Additionally, similar alteration assemblages occur in both hanging-wall and footwall facies of all three deposits (e.g., Peter et al., 2007; Bradshaw et al., 2008; Denisová, unpub. data).

The Finlayson Lake district has deposits with Zn tonnages up to 18.1 Mt (e.g., Kudz Ze Kayah) and Zn grades up to 9.66% (e.g., Wolverine) that are similar to many world-class VMS districts (Piercey et al., 2015), including districts with similar tectonostratigraphy and with deposits that commonly display features of replacement-style mineralization (e.g., Mount Read Volcanics, Skellefte district, and Iberian Pyrite Belt; Allen et al., 1996b, 2002; Large et al., 2001; Tornos, 2006).

Subseafloor replacement is a key process in the formation of large and high-grade VMS deposits (e.g., Rosebery, Tasmania and Kidd Creek, Ontario; Hannington et al., 1999; Martin, 2004), and recently SMS deposits (e.g., Hakurei Site, middle Okinawa Trough; Nozaki et al., 2021), because it enhances the amount of sulfide precipitated to increase the deposit tonnage, promotes higher degrees of preservation with increased burial in the ancient record, and facilitates zone refining processes during long-lived hydrothermal systems (Doyle and Allen, 2003; Piercey, 2015; Nozaki et al., 2021). All felsic-hosted VMS deposits in the Finlayson Lake district show abundant evidence for subseafloor replacement in both unconsolidated and coherent volcanic facies (e.g., Fig. 16), and our new U-Pb results, along with textural observations, indicate that they were hosted in facies sequences that were emplaced rapidly at both local and basin scales (>1,000 m/m.y.; e.g., Table 2). Rapid deposition of host lithofacies has been proposed as a diagnostic factor for facilitating replacement-style mineralization (Doyle and Allen, 2003); however, this attribute has been identified primarily by textural facies analysis and not with quantitative rates. There is significant variability in timing relative to volcano-sedimentary deposition for replacement-style deposits, where hydrothermal activity can be pre-, syn-, and post-deposition relative to the volcano-sedimentary sequence (e.g., Goodfellow and Franklin, 1993; Allen et al., 1996a, b; Hannington et al., 1999; Thurston et al., 2008; Belford et al., 2015). Subseafloor replacement is recognized at Middle Valley on Juan de Fuca Ridge, where sediment thicknesses and sedimentation rates are well-defined and indicate that hydrothermal sediment is absent below ~80 cm depth; this is interpreted to represent high sedimentation rates and subsidence prior to hydrothermal activity in the active vent sites (Goodfellow and Franklin, 1993). Further, Goodfellow and Franklin (1993) identified slower sediment accumulation rates at bathymetric highs compared to lows, which they suggest is due to shedding of sulfide mounds and clastic sediments into depressions because of tectonic and/or paleoslope instability related to movement on active rift-related normal faults. This relationship of sediment thickness, rate, and mineralization is also evident at a larger scale within the Kudz Ze Kayah formation despite a much larger volcanic component, where the Kudz Ze Kayah and GP4F deposits are spatially associated with the thickest and highest accumulation rates of volcaniclastic facies in the basin (Figs. 4, 8). Therefore, this comparison shows that localization of replacement-style deposits is related to both the thickest and most rapid rates of volcano-sedimentary accumulation.

We argue that rapid volcano-sedimentary accumulation rates are required to deposit volcano-sedimentary lithofacies with the infrastructure (i.e., porosity and permeability) for seawater (+hydrothermal fluid) infiltration that can then sustain the formation of large-tonnage and/or high-grade VMS deposits through zone refining processes and enhanced preservation. Continued rapid emplacement of lithofacies, particularly poorly sorted volcaniclastic mass-flows, as observed in the Kudz Ze Kayah and Wolverine deposits and their host stratigraphy, will both bury and preserve existing subseafloor mineralization and provide new substrate that has the potential to be mineralized. Rapid facies emplacement in these basins was likely an important factor for consistently developing

Fig. 16. Textural evidence for replacement-style mineralization in the Wolverine (A-C), GP4F (D-F), and Kudz Ze Kayah VMS deposits (G-L) in the Finlayson Lake VMS district. A) Primary shale fragments and beds that are replaced partially and fully to Zn-Pb sulfides, grading into massive sphalerite-pyrite-galena-sulfosalt assemblages. B) Massive Cu-Fe–rich sulfides that have replaced shale beds and tuff beds and fragments. C) Quartz-feldspar porphyritic rhyolite that has been fractured and replaced by sulfide veins. D) Chlorite-garnet–rich rock that is replaced by pyrite-pyrrhotite-sphalerite-galena assemblages, leaving rhyolite and lapilli clasts behind. E) Crystal tuff that has been variably replaced by sphalerite-pyrite ± pyrrhotite. F) Lapilli tuff with pyrite-pyrrhotite beds subparallel to tuff beds, where lapilli are preserved as fragments in the sulfides. G) Massive pyrite-pyrrhotite that replaces a coherent rhyolite flow. H) Sphalerite in fractures in a rhyolite flow. I) Remnant lapilli and feldspar crystals in massive pyrite-pyrrhotite-sphalerite beds. J) Massive pyrite ± sphalerite that contains remnant rhyolite clasts and tuff beds. K) Remnant lapilli fragments in pyrite-pyrrhotite-sphalerite-galena assemblage, grading down into chalcopyrite-rich section that replaces tuffs. L) Discordant replacement of coherent rhyolite with sphalerite-pyrite-pyrrhotite. Abbreviations: cpy = chalcopyrite, fsp = feldspar, gal = galena, grt = garnet, po = pyrrhotite, py = pyrite, qtz = quartz, rhy = rhyolite, sph = sphalerite, ss = sulfosalt.

thick accumulations of fertile lithofacies at the seafloor interface that are porous, permeable, and water saturated. Therefore, accumulation rates influenced the scale of hydrothermal mixing with seawater and resulted in the increased tonnages and high Zn grades found in all three felsic-hosted VMS deposits in the Finlayson Lake district.

Rapidly emplaced volcanic and volcano-sedimentary facies were previously argued to be important for facilitating subseafloor replacement-style VMS mineralization (Doyle and Allen, 2003); however, documentation of the actual emplacement rates of associated volcanic sequences has heretofore been inadequate and unquantified. Our approach underscores the significance of modern high-precision U-Pb geochronology to resolve rates and timescales of emplacement for VMS-related lithofacies in the ancient record. It is only with this enhanced high-resolution geochronology, coupled with detailed stratigraphic reconstructions and facies analysis, that we can more precisely unravel the governing factors between facies deposition, rates of emplacement, and mineralization styles that define high-value VMS deposits (i.e., high grade and/or tonnage) and most prospective basins in convergent margins globally.

## Conclusions

New high-precision U-Pb geochronological constraints on felsic volcanic rocks in the Finlayson VMS district provide well-constrained limits on the age of volcanism and associated VMS mineralization. The Kudz Ze Kayah formation is dominated by volcaniclastic and lesser subvolcanic and sedimentary facies that were erupted or deposited between 363.3 and 362.4 Ma ($\Delta t$ = 0.6–1.0 m.y.). In contrast, the Wolverine Lake group began sedimentary deposition at ca. 357.5 Ma, which then transitioned into a period of voluminous interbedded volcanic and argillite facies between 356.4 and 354.9 Ma ($\Delta t$ = 1.2–1.5 m.y.). These results indicate that the facies comprising the Kudz Ze Kayah formation and Wolverine Lake group were formed at rapid, time-averaged accumulation rates of ~300 to 1,900 m/m.y. (up to 2,900 m/m.y.) and ~800 to 1,400 m/m.y. (up to 7,800 m/m.y.), respectively, where the highest rates are interpreted to result from mass transport complex- or turbidity current-related deposition. Numerous subseafloor replacement-style VMS deposits are observed and documented in each of the geologic units and occur at distinct time intervals (GP4F = 363.3 Ma; Kudz Ze Kayah = 362.8 Ma; Wolverine = 355.2 Ma). We suggest that the thick, rapidly emplaced volcano-sedimentary facies in the Finlayson Lake district created a fertile, water-saturated environment that facilitated subseafloor replacement-style mineralization, rapidly covered the deposits, and thus enhanced their preservation and enabled zone refining in these subseafloor systems, all of which led to the development of VMS deposits with elevated Zn grades and tonnages. Together, high-precision geochronology, stratigraphic reconstructions, and detailed facies analysis can greatly improve our understanding of the rates, timescales, and characteristics of volcanism and associated VMS mineralization that produced the world-class VMS deposits in ancient convergent margins worldwide.

## Acknowledgments

## REFERENCES

Allen, C.M., and Campbell, I.H., 2012, Identification and elimination of a matrix-induced systematic error in LA–ICP–MS $^{206}$Pb/$^{238}$U dating of zircon: Chemical Geology, v. 332–333, p. 157–165.

Allen, R.L., Lundström, I., Ripa, M., Simeonov, A., and Christofferson, H., 1996a, Facies analysis of a 1.9 Ga, continental margin, back-arc, felsic caldera province with diverse Zn-Pb-Ag-(Cu-Au) sulfide and Fe oxide deposits, Bergslagen Region, Sweden: Economic Geology, v. 91, p. 979–1006.

Allen, R.L., Weihed, P., and Svenson, S.A., 1996b, Setting of Zn-Cu-Au-Ag massive sulfide deposits in the evolution and facies architecture of a 1.9 Ga marine volcanic arc, Skellefte district, Sweden: Economic Geology, v. 91, p. 1022–1053.

Allen, R.L., Weihed, P., Blundell, D., Crawford, T., Davidson, G., Galley, A.G., Gibson, H.L., Hannington, M.D., Herrington, R.J., Herzig, P.M., Large, R.R., Lentz, D.R., Maslennikov, V.V., McCutcheon, S.R., Peter, J.M., and Tornos, F., 2002, Global comparisons of volcanic-associated massive sulphide districts: Geological Society, London, Special Publications, v. 204, p. 13–37.

Allen, S.R., and Stewart, A.L., 2003, Products of explosive subaqueous felsic eruptions based on examples from the Hellenic Island Arc, Greece: American Geophysical Union, Geophysical Monograph 140, p. 285–298.

Arai, R., Kodaira, S., Yuka, K., Takahashi, T., Miura, S., and Kaneda, Y., 2017, Crustal structure of the southern Okinawa Trough: Symmetrical rifting, submarine volcano, and potential mantle accretion in the continental back-arc basin: Journal of Geophysical Research: Solid Earth, v. 122, p. 622–641.

Barrie, C.T., Cathles, L.M., Erendi, A., Schwaiger, H., and Murray, C., 1999, Heat and fluid flow in volcanic-associated massive sulfide-forming hydrothermal systems: Reviews in Economic Geology, v. 8, p. 201–220.

Belford, S.M., Davidson, G.J., McPhie, J., and Large, R.R., 2015, Architecture of the Neoarchaean Jaguar VHMS deposit, Western Australia: Implications for prospectivity and the presence of depositional breaks: Precambrian Research, v. 260, p. 136–160.

Bleeker, W., and Parrish, R.R., 1996, Stratigraphy and U-Pb zircon geochronology of Kidd Creek: Implications for the formation of giant volcanogenic massive sulphide deposits and the tectonic history of the Abitibi greenstone belt: Canadian Journal of Earth Sciences, v. 33, p. 1213–1231.

Bleeker, W., Parrish, R.R., and Sager-Kinsman, S., 1999, High-precision U-Pb geochronology of the Late Archean Kidd Creek deposit and surrounding Kidd volcanic complex: Economic Geology, Monograph 10, p. 43–69.

Bowring, J.F., McLean, N.M., and Bowring, S.A., 2011, Engineering cyber infrastructure for U-Pb geochronology: Tripoli and U-Pb-Redux: Geochemistry, Geophysics, Geosystems, v. 12, p. 1–19.

Bradshaw, G.D., Rowins, S.M., Peter, J.M., and Taylor, B.E., 2008, Genesis of the Wolverine volcanic sediment-hosted massive sulfide deposit, Finlayson Lake District, Yukon, Canada: Mineralogical, mineral chemical, fluid inclusion, and sulfur isotope evidence: Economic Geology, v. 103, p. 35–60.

Bryan, S.E., Peate, I.U., Peate, D.W., Self, S., Jerram, D.A., Mawby, M.R., Marsh, J.S.G., and Miller, J.A., 2010, The largest volcanic eruptions on Earth: Earth-Science Reviews, v. 102, p. 207–229.

Carey, S., 1999, Volcaniclastic sedimentation around island arcs, *in* Sigurdsson, H., Houghton, B.F., McNutt, S.R., Rymer, H., and Stix, J., eds.,

Encyclopedia of volcanoes (first edition): San Diego, Academic Press, p. 627–642.

Carey, S., and Sigurdsson, H., 1984, A model of volcanogenic sedimentation in marginal basins: Geological Society, London, Special Publications, v. 16, p. 37–58.

Cas, R.A.F., and Simmons, J.M., 2018, Why deep-water eruptions are so different from subaerial eruptions: Frontiers in Earth Science, v. 6, p. 1–21.

Cas, R.A.F., and Wright, J.V., 1987, Volcanic successions: Modern and ancient: London, Allen & Unwin, 528 p.

Catanzaro, E.J., Murphy, T.J., Shields, W.R., and Garner, E.L., 1968, Absolute isotopic abundance ratios of common, equal-atom, and radiogenic lead isotopic standards: Journal of Research of the National Bureau of Standards Section A: Physics and Chemistry, v. 72A, p. 261–267.

Cathles, L.M., Erendi, A.H.J., and Barrie, T., 1997, How long can a hydrothermal system be sustained by a single intrusive event?: Economic Geology, v. 92, p. 766–771.

Clift, P.D., 1995, Volcaniclastic sedimentation and volcanism during the rifting of western Pacific backarc basin: Active margins and marginal basins of the western Pacific: American Geophysical Union, Geophysical Monograph 88, p. 67–96.

Colpron, M., and Nelson, J., 2011, A digital atlas of terranes for the Northern Cordillera: Yukon Geological Survey, www.geology.gov.yk.ca.

Colpron, M., Nelson, J.L., and Murphy, D.C., 2006, A tectonostratigraphic framework for the pericratonic terranes of the northern Canadian Cordillera: Geological Association of Canada, Special Paper 45, p. 1–23.

Condon, D.J., Schoene, B., McLean, N.M., Bowring, S.A., and Parrish, R.R., 2015, Metrology and traceability of U-Pb isotope dilution geochronology (EARTHTIME Tracer Calibration Part I): Geochimica et Cosmochimica Acta, v. 164, p. 464–480.

Davydov, V.I., Crowley, J.L., Schmitz, M.D., and Poletaev, V.I., 2010, High-precision U-Pb zircon age calibration of the global Carboniferous time scale and Milankovitch band cyclicity in the Donets Basin, eastern Ukraine: Geochemistry, Geophysics, Geosystems, v. 11, p. 1–22.

Devine, F., Carr, S.D., Murphy, D.C., Davis, W.J., Smith, S., and Villeneuve, M., 2006, Geochronological and geochemical constraints on the origin of the Klatsa metamorphic complex: Implications for Early Mississippian high-pressure metamorphism within Yukon-Tanana terrane: Geological Association of Canada, Special Paper 45, p. 107–130.

Díaz-Asencio, M., Bartrina, V.F., and Herguera, J.C., 2019, Sediment accumulation patterns on the slopes and abyssal plain of the southern Gulf of Mexico: Deep-Sea Research Part I, v. 146, p. 11–23.

Doyle, M.G., and Allen, R.L., 2003, Subsea-floor replacement in volcanic-hosted massive sulfide deposits: Ore Geology Reviews, v. 23, p. 183–222.

Fisher, R.V., 1966, Rocks composed of volcanic fragments and their classification: Earth Science Reviews, v. 1, p. 287–298.

Franklin, J.M., Gibson, H.L., Jonasson, I.R., and Galley, A.G., 2005, Volcanogenic massive sulfide deposits: Economic Geology, 100th Anniversary Volume, p. 523–560.

Gabrielse, H., Murphy, D.C., and Mortensen, J.K., 2006, Cretaceous and Cenozoic dextral orogen-parallel displacements, magmatism, and paleogeography, north-central Canadian Cordillera: Geological Association of Canada, Special Paper 46, p. 255–276.

Gerstenberger, H., and Haase, G., 1997, A highly effective emitter substance for mass spectrometric Pb isotope ratio determinations: Chemical Geology, v. 136, p. 309–312.

Gibson, H.L., 2005, Volcano-hosted ore deposits, in Martí, J., and Ernst, G.G.J., eds., Volcanoes and the environment: Cambridge, Cambridge University Press, p. 333–386.

Gibson, H.L., Morton, R.L., and Hudak, G.J., 1999, Submarine volcanic processes, deposits, and environments favorable for the location of volcanic-associated massive sulfide deposits: Reviews in Economic Geology, v. 8, p. 13–52.

Goodfellow, W.D., and Franklin, J.M., 1993, Geology, mineralogy, and chemistry of sediment-hosted clastic massive sulfides in shallow cores, Middle Valley, Northern Juan de Fuca Ridge: Economic Geology, v. 88, p. 2037–2068.

Grant, S.L., 1997, Geochemical, radiogenic tracer isotopic, and U-Pb geochronological studies of Yukon-Tanana terrane rocks from the Money klippe, southeastern Yukon, Canada: M.Sc. thesis, Edmonton, Canada, University of Alberta, 177 p.

Hannington, M.D., Bleeker, W., and Kjarsgaard, I., 1999, Sulfide mineralogy, geochemistry and ore genesis of the Kidd Creek deposit: Part I. North, Central, and South orebodies: Economic Geology, Monograph 10, p. 163–224.

Hannington, M.D., De Ronde, C.E.J., and Petersen, S., 2005, Sea-floor tectonics and submarine hydrothermal systems: Economic Geology, 100th Anniversary Volume, p. 111–141.

Heuret, A., and Lallemand, S., 2005, Plate motions, slab dynamics and back-arc deformation: Physics of the Earth and Planetary Interiors, v. 149, p. 31–51.

Hudak, G.J., Morton, R.L., Franklin, J.M., and Peterson, D.M., 2003, Morphology, distribution, and estimated eruption volumes for intracaldera felsic tuff deposits in the Archean Sturgeon Lake subaqueous caldera complex, Northwestern Ontario: American Geophysical Union, Geophysical Monograph 140, p. 345–360.

Jaffey, A.H., Flynn, K.F., Glendenin, L.E., Bentley, W.C., and Essling, A.M., 1971, Precision measurement of half-lives and specific activities of $U^{235}$ and $U^{238}$: Physical Review C, v. 4, p. 1889–1906.

Jamieson, J.W., Clague, D.A., and Hannington, M.D., 2014, Hydrothermal sulfide accumulation along the Endeavour Segment, Juan de Fuca Ridge: Earth and Planetary Science Letters, v. 395, p. 136–148.

Karig, D.E., and Moore, G.F., 1975, Tectonically controlled sedimentation in marginal basins: Earth and Planetary Science Letters, v. 26, p. 233–238.

Kokelaar, P., and Busby, C., 1992, Subaqueous explosive eruption and welding of pyroclastic deposits: Science, v. 257, p. 196–201.

Krogh, T.E., 1973, A low-contamination method for hydrothermal decomposition of zircon and extraction of U and Pb for isotopic age determinations: Geochimica et Cosmochimica Acta, v. 87, p. 485–494.

Large, R.R., McPhie, J., Gemmell, J.B., Herrmann, W., and Davidson, G.J., 2001, The spectrum of ore deposit types, volcanic environments, alteration halos, and related exploration vectors in submarine volcanic successions: Some examples from Australia: Economic Geology, v. 96, p. 913–938.

le Friant, A., Deplus, C., Boudon, G., Sparks, R.S.J., Trofimovs, J., and Talling, P., 2009, Submarine deposition of volcaniclastic material from the 1995-2005 eruptions of Soufrière Hills volcano, Montserrat: Journal of the Geological Society, v. 166, p. 171–182.

Ludwig, K.R., 2003, Isoplot 3.09: A geochronological toolkit for Microsoft Excel: Berkeley Geochronology Center, Special Publication no. 4, 74 p.

MacRobbie, P., and Holroyd, R.W., 2000, 1998 and 1999 Year End Report, TAG Property (KZK Project), Cominco Ltd. Exploration Canada: Unpublished internal report, 41 p.

Marsaglia, K.M., Boggs, S., Clift, P., Seyedolali, A., and Smith, R., 1995, Sedimentation in western pacific backarc basins: New insights from recent ODP drilling: American Geophysical Union, Geophysical Monograph 88, p. 291–314.

Martin, N.K., 2004, Genesis of the Rosebery massive sulphide deposit, western Tasmania, Australia: Ph.D. dissertation, Hobart, Australia, University of Tasmania, 273 p.

Mathur, R., Ruiz, J., and Tornos, F., 1999, Age and sources of the ore at Tharsis and Rio Tinto, Iberian pyrite belt, from Re-Os isotopes: Mineralium Deposita, v. 34, p. 790–793.

Mattinson, J.M., 2005, Zircon U-Pb chemical abrasion ("CA-TIMS") method: Combined annealing and multi-step partial dissolution analysis for improved precision and accuracy of zircon ages: Chemical Geology, v. 220, p. 47–66.

Mckenzie, D., and Bickle, M.J., 1988, The volume and composition of melt generated by extension of the lithosphere: Journal of Petrology, v. 29, p. 625–679.

McLean, N.M., Condon, D.J., Schoene, B., and Bowring, S.A., 2015, Evaluating uncertainties in the calibration of isotopic reference materials and multi-element isotopic tracers (EARTHTIME Tracer Calibration Part II): Geochimica et Cosmochimica Acta, v. 164, p. 481–501.

McPhie, J., and Allen, R.L, 1992, Facies architecture of mineralized submarine volcanic sequences: Cambrian Mount Read Volcanics, western Tasmania: Economic Geology, v. 87, p. 587–596.

McPhie, J., Doyle, M.G., and Allen, R.L., 1993, Volcanic textures: A guide to interpretation of textures in volcanic rocks: Hobart, University of Tasmania, 198 p.

Minami, H., Nagasawa, R., and Ohara, Y., 2020, Detailed volcanic and tectonic morphology of Nakadomari Hill in the southern Okinawa Trough: Marine Geology, v. 421, article 106094.

Mortensen, J.K., 1983, Age and evolution of the Yukon- Tanana terrane, southeastern Yukon Territory: Ph.D. dissertation, Santa Barbara, University of California, 115 p.

——1992, Pre-Mid-Mesozoic tectonic evolution of the Yukon-Tanana Terrane, Yukon and Alaska: Tectonics, v. 11, p. 836–853.

Mortensen, J.K., and Jilson, G.A., 1985, Evolution of the Yukon-Tanana terrane: Evidence from southeastern Yukon Territory: Geology, v. 13, p. 806–810.

Mortensen, J.K., Gemmell, J.B., McNeill, A.W., and Friedman, R.M., 2015, High-precision U-Pb zircon chronostratigraphy of the Mount Read Volcanic Belt in Western Tasmania, Australia: Implications for VHMS deposit formation: Economic Geology, v. 110, p. 445–468.

Murphy, D.C., and Piercey, S.J., 1999, Finlayson project: Geological evolution of Yukon-Tanana Terrane and its relationship to Campbell Range belt, northern Wolverine Lake map area, southeastern Yukon, in Roots, C.F., and Emond, D.S., eds., Yukon exploration and geology 1998: Exploration and Geological Services Division, Yukon Region, Indian and Northern Affairs Canada, p. 47–62.

Murphy, D.C., Colpron, M., Roots, C.F., Gordey, S.P., and Abbott, J.G., 2002, Finlayson Lake targeted geoscience initiative (southeastern Yukon), part 1: Bedrock geology, in Emond, D.S., Weston, L.H., and Lewis, L.L., eds., Yukon exploration and geology 2001: Exploration and Geological Services Division, Yukon, Indian and Northern Affairs Canada, p. 189–207.

Murphy, D.C., Mortensen, J.K., Piercey, S.J., Orchard, M.J., and Gehrels, G.E., 2006, Mid-Paleozoic to early Mesozoic tectonostratigraphic evolution of Yukon-Tanana and Slide Mountain terranes and affiliated overlap assemblages, Finlayson Lake massive sulphide district, southeastern Yukon: Geological Association of Canada, Special Paper 45, p. 75–106.

Nasdala, L., Lengauer, C.L., Hanchar, J.M., Kronz, A., Wirth, R., Blanc, P., Kennedy, A.K., and Seydoux-Guillaume, A.M., 2002, Annealing radiation damage and the recovery of cathodoluminescence: Chemical Geology, v. 191, p. 121–140.

Nesbitt, R.W., Pascual, E., Fanning, C.M., Toscano, M., Saes, R., and Almodovar, G.R., 1999, U-Pb dating of stockwork zircons from the eastern Iberian Pyrite Belt: Journal of the Geological Society, London, v. 156, p. 7–10.

Nozaki, T., Kato, Y., and Suzuki, K., 2014, Re-Os geochronology of the Hitachi volcanogenic massive sulfide deposit: The oldest ore deposit in Japan: Economic Geology, v. 109, p. 2023–2034.

Nozaki, T., Nagase, T., Takaya, Y., Yamasaki, T., Otake, T., Yonezu, K., Ikehata, K., Totsuka, S., Kitada, K., Sanada, Y., Yamada, Y., Ishibashi, J., Kumagai, H., Maeda, L., and D/V Chikyu Expedition 909 Scientists, 2021, Subseafloor sulphide deposit formed by pumice replacement mineralisation: Scientific Reports, v. 11, p. 1–11.

Oliver, J., McNulty, B., and Friedman, R., 2021, High-precision CA-ID-TIMS age constraints on the Niblack Cu-Zn-Au-Ag deposits: A Neoproterozoic volcanic-hosted massive sulfide deposit in the North American Cordillera: Economic Geology, v. 116, p. 1467–1481.

Pedersen, R.B., Dunning, G.R., and Robins, B., 1989, U-Pb ages of nepheline syenite pegmatites from the Seiland Magmatic Province, N Norway, in Gayer, R.A., ed., The Caledonide geology of Scandinavia: London, Graham and Trotman, p. 3–8.

Peter, J.M., Layton-Matthews, D., Piercey, S.J., Bradshaw, G.D., Paradis, S,. and Bolton, A., 2007, Volcanic-hosted massive sulphide deposits of the Finlayson Lake District, Yukon: Geological Association of Canada, Mineral Deposits Division, Special Publication no. 5, p. 471–508.

Piercey, S.J., 2001, Petrology and tectonic setting of felsic and mafic volcanic and intrusive rocks in the Finlayson Lake volcanic-hosted massive sulphide (VHMS) district, Yukon, Canada: A record of mid-Paleozoic arc and back-arc magmatism and metallogeny: Ph.D. dissertation, Vancouver, Canada, University of British Columbia, 324 p.

——2011, The setting, style, and role of magmatism in the formation of volcanogenic massive sulfide deposits: Mineralium Deposita, v. 46, p. 449–471.

——2015, A semipermeable interface model for the genesis of subseafloor replacement-type volcanogenic massive sulfide (VMS) deposits: Economic Geology, v. 110, p. 1655–1660.

Piercey, S.J., and Colpron, M., 2009, Composition and provenance of the Snowcap assemblage, basement to the Yukon-Tanana terrane, northern Cordillera: Implications for Cordilleran crustal growth: Geosphere, v. 5, p. 439–464.

Piercey, S.J., Paradis, S., Murphy, D.C., and Mortensen, J.K., 2001, Geochemistry and paleotectonic setting of felsic volcanic rocks in the Finlayson Lake volcanic-hosted massive sulfide district, Yukon, Canada: Economic Geology, v. 96, p. 1877–1905.

Piercey, S.J., Mortensen, J.K., Murphy, D.C., Paradis, S., and Creaser, R.A., 2002, Geochemistry and tectonic significance of alkalic mafic magmatism in the Yukon-Tanana terrane, Finlayson Lake region, Yukon: Canadian Journal of Earth Sciences, v. 39, p. 1729–1744.

Piercey, S.J., Murphy, D.C., Mortensen, J.K., and Creaser, R.A., 2004, Mid-Paleozoic initiation of the northern Cordilleran marginal backarc basin: Geologic, geochemical, and neodymium isotope evidence from the oldest mafic magmatic rocks in the Yukon-Tanana terrane, Finlayson Lake district, southeast Yukon, Canada: Bulletin of the Geological Society of America, v. 116, p. 1087–1106.

Piercey, S.J., Nelson, J.L., Colpron, M., Dusel-bacon, C., Simard, R.-L., and Roots, C.F., 2006, Paleozoic magmatism and crustal recycling along the ancient Pacific margin of North America, northern Cordillera: Geological Association of Canada, Special Paper 45, p. 281–322.

Piercey, S.J., Peter, J.M., Mortensen, J.K., Paradis, S., Murphy, D.C., and Tucker, T.L., 2008, Petrology and U-Pb geochronology of footwall porphyritic rhyolites from the Wolverine volcanogenic massive sulfide deposit, Yukon, Canada: Implications for the genesis of massive sulfide deposits in continental margin environments: Economic Geology, v. 103, p. 5–33.

Piercey, S.J., Peter, J.M., and Herrington, R.J., 2015, Zn-rich volcanogenic massive sulphide (VMS) deposits, in Archibald, S.M., and Piercey, S.J., eds., Current perspectives on zinc deposits: Dublin, Irish Association for Economic Geology, p. 37–57.

Piercey, S.J., Gibson, H.L., Tardif, N., and Kamber, B.S., 2016, Ambient redox and hydrothermal environment of the Wolverine volcanogenic massive sulfide deposit, Yukon: Insights from lithofacies and lithogeochemistry of Mississippian host shales: Economic Geology, v. 111, p. 1439–1463.

Regan, M., 2007, Amended technical report on the Wolverine property: Yukon Zinc Corporation, National Instrument 43-101 Technical Report No. 0652630101-REP-R0004-02, 149 p.

Rioux, M., Lissenberg, C.J., McLean, N.M., Bowring, S.A., MacLeod, C.J., Hellebrand, E., and Shimizu, N., 2012, Protracted timescales of lower crustal growth at the fast-spreading East Pacific Rise: Nature Geoscience, v. 5, p. 275–278.

Ross, P.-S., McNicoll, V.J., Debreil, J.A., and Carr, P., 2014, Precise U-Pb geochronology of the Matagami mining camp, Abitibi greenstone belt, Quebec: Stratigraphic constraints and implications for volcanogenic massive sulfide exploration: Economic Geology, v. 109, p. 89–101.

Samperton, K.M., Schoene, B., Cottle, J.M., Keller, C.B., Crowley, J.L., and Schmitz, M.D., 2015, Magma emplacement, differentiation, and cooling in the middle crust: Integrated zircon geochronological-geochemical constraints from the Bergell Intrusion, central Alps: Chemical Geology, v. 417, p. 322–340.

Santschi, P.H., and Rowe, G.T., 2008, Radiocarbon-derived sedimentation rates in the Gulf of Mexico: Deep-Sea Research Part II, v. 55, p. 2572–2576.

Schmitz, M.D., and Davydov, V.I., 2012, Quantitative radiometric and biostratigraphic calibration of the Pennsylvanian-Early Permian (Cisuralian) time scale and pan-Euramerican chronostratigraphic correlation: Bulletin of the Geological Society of America, v. 124, p. 549–577.

Schmitz, M.D., and Schoene, B., 2007, Derivation of isotope ratios, errors, and error correlations for U-Pb geochronology using $^{205}Pb$-$^{235}U$-($^{233}U$)-spiked isotope dilution thermal ionization mass spectrometric data: Geochemistry, Geophysics, Geosystems, v. 8, 20 p., doi:10.1029/2006GC001492.

Schoene, B., 2014, U-Th-Pb geochronology, in Holland, H.D., and Turekian, K.K., eds., Treatise on geochemistry, v. 4, 2nd ed.: Oxford, Elsevier-Pergamon, v. 4, p. 341–378.

Schoene, B., and Baxter, E.F., 2017, Petrochronology and TIMS: Reviews in Mineralogy and Geochemistry, v. 83, p. 231–260.

Schoene, B., Crowley, J.L., Condon, D.J., Schmitz, M.D., and Bowring, S.A., 2006, Reassessing the uranium decay constants for geochronology using ID-TIMS U-Pb data: Geochimica et Cosmochimica Acta, v. 70, p. 426–445.

Sebert, C., Hunt, J.A., and Foreman, I.J., 2004, Geology and lithogeochemistry of the Fyre Lake copper-cobalt-gold sulphide-magnetite deposit, southeastern Yukon: Yukon Geological Survey, Open File 2004-17, 46 p.

Sillitoe, R.H., 2010, Porphyry copper systems: Economic Geology, v. 105, p. 3–41.

Sláma, J., Košler, J., Condon, D., Crowley, J., Gerdes, A., et al., 2008, Plešovice zircon—a new natural reference material for U-Pb and Hf isotopic microanalysis: Chemical Geology, v. 249, p. 1–35.

Tempelman-Kluit, D.J., 1979, Transported cataclasite, ophiolite and granodiorite in Yukon: Evidence of arc-continent collision: Geological Survey of Canada, Paper 79-14, 27 p.

Thurston, P.C., Ayer, J.A., Goutier, J., and Hamilton, M.A., 2008, Depositional gaps in Abitibi greenstone belt stratigraphy: A key to exploration for syngenetic mineralization: Economic Geology, v. 103, p. 1097–1134.

Tornos, F., 2006, Environment of formation and styles of volcanogenic massive sulfides: The Iberian Pyrite Belt: Ore Geology Reviews, v. 28, p. 259–307.

Tornos, F., Peter, J.M., Allen, R., and Conde, C., 2015, Controls on the siting and style of volcanogenic massive sulphide deposits: Ore Geology Reviews, v. 68, p. 142–163.

van Olden, K., Green, A., and Davidson, G., 2019, Kudz Ze Kayah Property, Yukon, Canada: BMC Minerals Ltd., National Instruments 43-101 Feasibility Study Technical Report R173.2019, 376 p., http://www.sedar.com/.

White, J.D.L., 2000, Subaqueous eruption-fed density currents and their deposits: Precambrian Research, v. 101, p. 87–109.

White, J.D.L., and Houghton, B.F., 2006, Primary volcaniclastic rocks: Geology, v. 34, p. 677–680.

White, S.M., Crisp, J.A., and Spera, F.J., 2006, Long-term volumetric eruption rates and magma budgets: Geochemistry, Geophysics, Geosystems, v. 7, doi: 10.1029/2005GC001002.

Wotzlaw, J.F., Schaltegger, U., Frick, D.A., Dungan, M.A., Gerdes, A., and Günther, D., 2013, Tracking the evolution of large-volume silicic magma reservoirs from assembly to supereruption: Geology, v. 41, p. 867–870.

Yukon Geological Survey, 2018, Yukon digital bedrock geology: http://www.geology.gov.yk.ca/update_yukon_bedrock_geology_map.html.



**Matthew Manor** recently graduated with a Ph.D. from Memorial University of Newfoundland. He completed his B.Sc. at the University of Minnesota Duluth in 2012 and his M.Sc. at the University of British Columbia (UBC) in 2014. Matthew's research integrates field mapping, petrology, lithogeochemistry, and U-Pb geochronology in both magmatic and hydrothermal ore deposit systems. His current work focuses on combined bulk-rock and in situ geochronology and geochemistry of felsic rocks in the Finlayson Lake VMS district, Yukon, to define new prospectivity criteria for VMS exploration and provide new insights on the global-scale interplay of tectonics, magmatism, and VMS genesis.